Mathematics in Applied Sciences and Engineering
Volume **6**, Number **2**, June **2025**, pp.**174-202**

https://ojs.lib.uwo.ca/mase
https://doi.org/10.5206/mase/22320

ANALYSIS OF LINEAR CAPILLARY GRAVITY WAVE SCATTERING BY A SUBMERGED PLATE OVER AN ASYMMETRICAL TRENCH

MAMPI MAJHI AND RUMPA CHAKRABORTY

Abstract. To protect a harbor from the open sea, one can consider a sustainable construction of breakwater in the form of a submerged vertical thin barrier over an asymmetric rectangular trench. In the present study, the scattering of water waves by submerged vertical breakwater over an asymmetric trench in the presence of capillary gravity wave interaction is considered. Applying linear theory, the scattering problem is investigated in the case of three different positions of a fully submerged barrier in the presence of surface tension. The mathematical problem is structured in terms of integral equations which are operated by using two different numerical approaches, The first one is the Boundary element method and the second one is the multi-term Galerkin Approximation technique where the basis functions are chosen in terms of ultraspherical Gegenbauer polynomials and Chebychev polynomials for the different singularities at the edge of the trench and the barrier respectively. These techniques aid in reducing the integral equation to a system of algebraic equations and they are solved for unknowns. The comparison between the results obtained from the two different techniques is given. Besides, choosing an orthogonal polynomial, one can also choose a simple polynomial as a basis function in Galerkin technique. In the present study, a better convergence rate is given by orthogonal polynomials than simple ones. The effectiveness of the vertical submerged breakwater over an asymmetric trench in the presence of surface tension is studied by analyzing the numerical results for different physical quantities like reflection, transmission coefficients, and wave load which are depicted graphically against wave number. Comparisons between present results and experimental results are shown graphically for reflection and transmission coefficients.

1. Introduction

Capillary-gravity waves are mainly surface waves in the region where the restoring effect of both capillary and gravity waves are equal in magnitude. These waves interaction can be seen in the water-air interface which causes generation of wind ripples at the ocean surface [38]. These waves can be identified by some satellite sensors and used to control remote sensing of the ocean surface. These also provide early warning for applications such as marine pollution, spread of harmful angal blooms or findings oil spills [36]. In the presence of a capillary-gravity wave, the characteristics of associated water wave motion are dominated by surface tension. The amplitude and frequency of the wave depend on both the surface tension and gravity but usually the surface tension is commonly ignored in describing water waves around large floating bodies. Its effect is considered only for short waves. The surface tension of fresh water is generally known as $71.97mN/m$, this value increases because of the presence of iodized salts, different minerals, ions etc. for sea water, and varies within $72.9mN/m - 75mN/m$. However, the theory of gravity waves may produce very short lengthen wave that cannot be ignored and cause substantial difficulties in modelling them. These singular and highly oscillatory properties

Received by the editors 2 January 2025; accepted 9 April 2025; published online 5 June 2025.

2020 *Mathematics Subject Classification.* 76B15.

Key words and phrases. Water wave scattering, asymmetric trench, surface tension, multi-term Galerkin approximation, orthogonal and simple polynomials, reflection and transmission coefficients.

are obviously not tangible, it is expected that the surface tension plays an important role in modelling surface waves [24].

In linear theory, it becomes crucial to understand the physical interpretation of an existential of coherent structures in the dynamics of the capillary-gravity wave. Here the structure is considered as a submerged vertical barrier. These also can consider as a breakwater in oceans. Many researchers are already discussed scattering problems involving fully submerged barrier present in finite-depth water. Diffraction of water waves by a submerged vertical plate is analyzed by Evans [6]. Parsons and Martin presented an analytical solution for water waves by submerged plates. The problem is formulated in terms of a hypersingular integral equation and solved by using Green's integral theorem [25]. Later they extended their work considering the scattering by submerged, curved plates and also by surface-piercing, flat plates [26]. The effect of surface tension on the reflection of waves is observed by Evans [5] in the presence of a vertical surface piercing a rigid barrier at first. Rhodes-Robinson [31] studied the problem of surface tension in the water of infinite depth by complex variable method. Hogan [10] investigated deep water capillary gravity waves and stated that even for long wavelength waves surface tension should be included. Chen [4] gave an updated analysis on the steady ship waves including the effect of surface tension.

Sometimes it is more effective as a breakwater if we add a thin submerged barrier over the trench. Due to various applications in coastal and ocean engineering, for example, to disseminate waves and reduce their energy before they reach the shoreline. This can help to guard seaside areas, building construction, and other coastal infrastructures from the destructive impacts of oceanic waves. Trenches can also be used in water treatment systems to allow sedimented sludge and other particles to settle out of the water. All these physical applications are encouraged in studying such problems. First Kreisel [17] reduced the fluid domain to a rectangular strip using an appropriate conformal mapping and then converted the boundary value problem of the potential function into an integral equation. Lassiter [18] examined the scattering of normally incident monochromatic plane progressive waves by a rectangular submarine trench where the water depths are constants before and after trench but not equal. Mei and Black [22] obtained the numerical estimation for the reflection coefficient for water wave scattering by a bottom-standing thick rectangular barrier. The effect of a symmetric rectangular trench by dividing the fluid domain into two subregions and obtained expressions for the velocity potentials for each subregion by matching procedure investigated by Lee and Ayer [19]. Miles [23] applied a conformal mapping to solve the trench problem for normal incidence of the wave train. Kirby and Dalrymple [16] also considered problem of obliquely incident waves over an asymmetric trench for which the water depths in its two sides are unequal but constant. Utilizing matching eigenfunction expansions of the velocity potentials, they solved a set of integral equations for each subregion of constant depth along two vertical boundaries and compared the numerical results with the obtained data from experiments. The problem of wave propagation over two-dimensional trenches and shoals are considered by Bender and Dean [1] by employing three solution methods that are the step method valid in arbitrary depths of water and the slope method and the numerical method which are valid in shallow water regions. Xie et al. [37] have been used to develop the reflection coefficient in a closed form by using first and second-kind Bessel functions in the problem of long-wave reflection by a rectangular obstacle with two scour trenches of power function profile. Later, Liu et al. [20] investigated the problem of a rectangular breakwater with two scour trenches by employing a modified mild-slope equation and the reflection coefficient was obtained analytically. Jung et al [11] studied the analytical solutions for waves propagating over an asymmetric trench using power series technique. Other studies that include the effect of surface tension in the field of water waves can be seen in Sasmal and De [35].

Galerkin method is very useful technique to operate different water wave problems. Earlier, Evans and Morris [7], Evans and Fernyhough [8], Porter and Evans [27] used Galerkin approximation technique followed by Havelock's [9] expansion of water wave potential to obtain numerical estimates for the reflection coefficient for oblique incidence of the wave train on a single vertical barrier in deep and finite depth water. Roy et al. [28] investigated the problem of water wave scattering over an asymmetric rectangular trench. Sarkar et al. [34] also employed the multiterm Galerkin approximation to solve the problem of oblique wave interaction by two thin vertical barriers over an asymmetric trench. Kanoria et al. [12] formulated the problem of water wave scattering by a thick vertical barrier of rectangular cross-section having four different geometrical shapes using multiterm Galerkin approximations involving ultraspherical Gegenbauer polynomials of order $\frac{1}{6}$. The normal and oblique incidence by the two-dimensional wave scattering by a rectangular submarine trench was considered by Chakraborty and Mandal [2, 3]. To solve integral equation, multi-term Galerkin approximation is used involving ultraspherical Gegenbauer polynomials. Using the boundary element method(BIM), Kar et al. [13] developed the problem of scattering of surface gravity waves over a pair of trenches. Kaur et al. [14] applied Galerkin method together with the polynomial as a basis function to solve the resulting singular integral equations. In addition, the boundary element method used to solve an integral equation is discussed in [32, 33]. Again, Kaur et. al. [15] used least-square method and singular value decomposition method to solve the algebraic equations in the problem of mitigation of wave energy by trench-type structure.

As per author's understanding, not much research have been done related to the problem of a submerged vertical rigid plate over a rectangular trench in presence of cohesive force at the upper surface of the water. In the following section, the problem of water wave scattering by a thin vertical fully submerged rigid barrier over an asymmetric trench with surface tension is investigated for different three positions. In first case, the barrier is put at position $x = 0$ in the trench; in second case, the barrier is placed on the right side from position $x = 0$ in the trench; in third case, the barrier is placed on the out side of the trench. Then for each position, the problem is reduced to first kind integral equations involving horizontal component of velocity potential which has a cube-root singularity near the corners of the trench and a square-root singularity near the edge of the vertical barrier. A new complete analytical solutions for present problem are developed by solving the integral equations utilizing multi-term Galerkin approximation method. A set of basis functions are chosen in terms of ultraspherical Gegenbauer and Chebychev's polynomials due to different singularities with suitable weights. Then numerical results for reflection, transmission coefficients and wave load are obtained and depicted graphically against the wave number and it is observed how surface tension affects them. The convergence of the newly growing analytical solutions is governed and the tabulated results are compared with the results of Lee and Ayer [19] and Kirby and Dalrymple [16] numerically. In both cases, good agreement is seen and these establish the correctness of numerical results. This signifies the correctness of the method employed here.

2. Problem Definition

The present problem is considered in a two-dimensional Cartesian coordinate system with a horizontal x-axis and the y-axis is chosen vertically downward. The fluid region is occupied in $y \geq 0$ in the presence of a rectangular trench of depth h_2 and width (b_1+b_3) associated with surface tension on the free surface. The fluid depth before and after the trench are different but constants h_1 and h_3, respectively. A thin vertical fully submerged barrier of length $a_2 - a_1$, is situated at $x = b_2$, when $b_2 = 0$, the barrier is at the position $x = 0$ of the trench (first case), secondly, the barrier is placed right from the position $x = 0$ of trench (second case) so that $b_2 < b_3$, and in the third case the barrier is shifted outside of the

trench at $x = b_2$ such that $b_2 > b_3$, which are shown in the sketch of FIGURE 1. Thus, the whole fluid domain is divided into four sub- regions such as

$$\begin{cases} R_1 : -\infty < x < -b_1, 0 < y < h_1, \\ R_2 : -b_1 < x < b_2, 0 < y < h_2, \quad \text{for case-I,II} \\ R_3 : b_2 < x < b_3, 0 < y < h_2, \\ R_4 : b_3 < x < \infty, 0 < y < h_3; \end{cases}$$

$$\begin{cases} R_1 : -\infty < x < -b_1, 0 < y < h_1, \\ R_2 : -b_1 < x < b_3, 0 < y < h_2, \quad \text{for case-III} \\ R_3 : b_3 < x < b_2, 0 < y < h_3, \\ R_4 : b_3 < x < \infty, 0 < y < h_3. \end{cases}$$

The fluid is assumed to be incompressible, inviscid and homogeneous and the motion of the fluid to be irrotational and simple harmonic with time. On the assumption of the linear theory of water waves, a normally incident wave train is constructed by the velocity potential function $Re[\phi^{inc}(x,y)e^{i\nu z - i\omega t}]$ where

$$\phi^{inc}(x,y) = \frac{\cosh \lambda_0^{(1)}(h_1 - y)\ e^{i\mu_1(x+b_1)}}{\cosh \lambda_0^{(1)} h_1} \tag{2.1}$$

with $\mu_1 = \lambda_0^{(1)} \cos\theta$, $\nu = \lambda_0^{(1)} \sin\theta$, θ being the angle of incident of the wave with positive x-axis and $\lambda_0^{(1)}$ is the wave number of incident wave and it is the unique real positive root of dispersion relation

$$\lambda(1 + M\lambda^2) \tanh \lambda h_1 = \frac{\omega^2}{g} \tag{2.2}$$

with $M = \frac{\tau}{\rho g}$, ω is the angular frequency of the incident wave and g is the acceleration due to gravity, τ is the coefficient of surface tension and ρ is the uniform fluid density. The projection of the incident wave satisfies $\nu = \lambda_0^{(2)} \sin\theta' = \lambda_0^{(3)} \sin\theta''$, where $\lambda_0^{(j)} (j = 2, 3)$ is the unique real positive root of dispersion relation $\lambda(1 + M\lambda^2) \tanh \lambda h_j = \frac{\omega^2}{g}$, θ' and θ'' being the refraction angles arises due to the Snell's law. Then the resulting velocity potential $Re[\phi^{inc}(x,y)e^{i\nu z - i\omega t}]$ where $\phi^{inc}(x,y)$ satisfies the modified Helmholz's equation, can be described its motion in the fluid domain along with boundary conditions.

$$(\nabla^2 - \nu^2)\phi = 0 \ \text{ in the fluid region} \tag{2.3}$$

the upper surface condition

$$M\frac{\partial^3 \phi}{\partial y^3} + \frac{\partial \phi}{\partial y} + \frac{\omega^2}{g}\phi = 0 \text{ on } y = 0\ , -\infty < x < \infty, \tag{2.4}$$

$$\phi_x = 0 \text{ on } \begin{cases} x = -b_1, h_1 < y < h_2, \\ x = 0, a_1 < y < a_2 \quad \text{(c.f. FIGURE 1(A))}, \\ x = b_2, a_1 < y < a_2 \quad \text{(c.f. FIGURE 1(B),1(C))}, \\ x = b_3, h_3 < y < h_2, \end{cases} \tag{2.5}$$

the bottom conditions are

$$\phi_y = 0 \text{ on } \begin{cases} y = h_1, -\infty < x < -b_1, \\ y = h_2, -b_1 < x < b_3, \\ y = h_3,\ b_3 < x < \infty, \end{cases} \tag{2.6}$$

while the edge conditions are

$$r_1^{\frac{1}{3}} \nabla\phi \text{ is bounded as } r_1 \to 0 \tag{2.7}$$

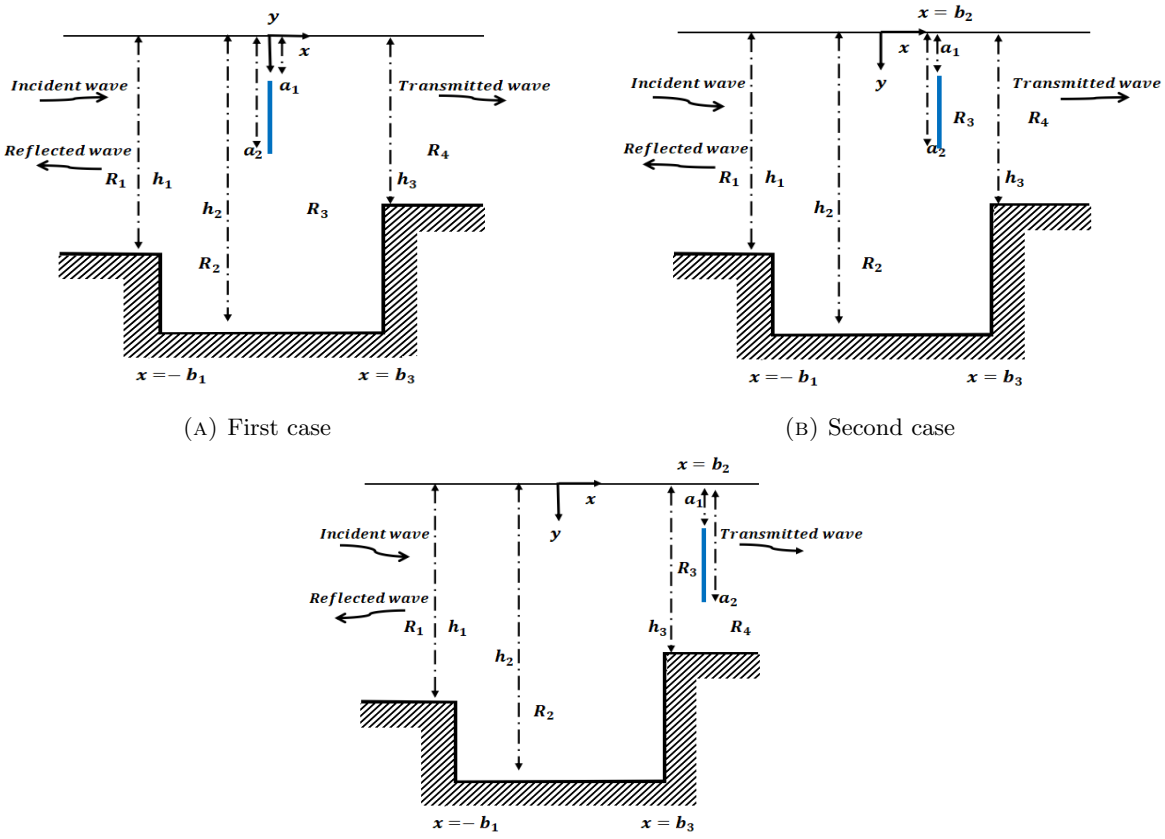

(A) First case

(B) Second case

(C) Third case

FIGURE 1. Schematic sketch of the trench along with vertically thin barrier.

where r_1 is the distance from the submerged sharp edge of the trench and

$$r_2^{\frac{1}{2}} \nabla \phi \text{ is bounded as } r_2 \to 0 \tag{2.8}$$

where r_2 is the distance from the submerged sharp edge of the barriers. The far-field behavior of the potential function is described by

$$\phi(x,y) \sim \begin{cases} \frac{\cosh \lambda_0^{(1)}(h_1-y)\ e^{i\mu_1(x+b_j)}}{\cosh \lambda_0^{(1)} h_1} + R\ \frac{\cosh \lambda_0^{(1)}(h_1-y)\ e^{-i\mu_1(x+b_j)}}{\cosh \lambda_0^{(1)} h_1} \text{ as } x \to -\infty,\ j = 1 \text{ for case-I,II,III,} \\ T\ \frac{\cosh \lambda_0^{(3)}(h_3-y)\ e^{i\mu_3(x-b_j)}}{\cosh \lambda_0^{(3)} h_3} \text{ as } x \to -\infty,\ \ j = 2 \text{ for case-I,II and } j = 3 \text{ for case-III,} \end{cases} \tag{2.9}$$

where $\mu_3 = \{(\lambda_0^{(3)})^2 - \nu^2\}^{\frac{1}{2}} = \lambda_0^{(3)} \sin\theta''$, R and T are the unknown constants associated with the reflection and transmission wave amplitude, respectively which are to be determined.

3. Method of solution

Now the velocity potential $\phi(x,y)$ for different regions can be expressed as for case-I,II

$$\phi(x,y)\sim\begin{cases}\frac{\cosh\lambda_0^{(1)}(h_1-y)}{\cosh\lambda_0^{(1)}h_1}\left[e^{i\mu_1(x+b_1)}+Re^{-i\mu_1(x+b_1)}\right]+\sum_{n=1}^{\infty}A_n\frac{\cos\lambda_n^{(1)}(h_1-y)}{\cos\lambda_n^{(1)}h_1}e^{s_n^{(1)}(x+b_1)} & \text{in } R_1,\\ \left[B_0\cos\mu_2(x+b_1)+C_0\sin\mu_2(x-b_2)\right]\frac{\cosh\lambda_0^{(2)}(h_2-y)}{\cosh\lambda_0^{(2)}h_2}\\ +\sum_{n=1}^{\infty}\left[B_n\cosh\{s_n^{(2)}(x+b_1)\}+C_n\sinh s_n^{(2)}(x-b_2)\right]\frac{\cos\lambda_n^{(2)}(h_2-y)}{\cos\lambda_n^{(2)}h_2} & \text{in } R_2,\\ \left[D_0\cos\mu_2(x-b_2)+E_0\sin\mu_2(x-b_3)\right]\frac{\cosh\lambda_0^{(2)}(h_2-y)}{\cosh\lambda_0^{(2)}h_2}\\ +\sum_{n=1}^{\infty}\left[D_n\cosh s_n^{(2)}(x-b_2)+E_n\sinh\{s_n^{(2)}(x-b_3)\}\right]\frac{\cos\lambda_n^{(2)}(h_2-y)}{\cos\lambda_n^{(2)}h_2} & \text{in } R_3,\\ \frac{\cosh\lambda_0^{(3)}(h_3-y)}{\cosh\lambda_0^{(3)}h_3}Te^{i\mu_3(x-b_3)}+\sum_{n=1}^{\infty}F_n\frac{\cos\lambda_n^{(3)}(h_3-y)}{\cos\lambda_n^{(3)}h_3}e^{s_n^{(3)}(x-b_3)} & \text{in } R_4;\end{cases}\tag{3.1}$$

and for case-III

$$\phi(x,y)\sim\begin{cases}\frac{\cosh\lambda_0^{(1)}(h_1-y)}{\cosh\lambda_0^{(1)}h_1}\left[e^{i\mu_1(x+b_1)}+Re^{-i\mu_1(x+b_1)}\right]+\sum_{n=1}^{\infty}A_n\frac{\cos\lambda_n^{(1)}(h_1-y)}{\cos\lambda_n^{(1)}h_1}e^{s_n^{(1)}(x+b_1)} & \text{in } R_1,\\ \left[B_0\cos\mu_2(x+b_1)+C_0\sin\mu_2(x-b_3)\right]\frac{\cosh\lambda_0^{(2)}(h_2-y)}{\cosh\lambda_0^{(2)}h_2}\\ +\sum_{n=1}^{\infty}\left[B_n\cosh\{s_n^{(2)}(x+b_1)\}+C_n\sinh s_n^{(2)}(x-b_3)\right]\frac{\cos\lambda_n^{(2)}(h_2-y)}{\cos\lambda_n^{(2)}h_2} & \text{in } R_2,\\ \left[D_0\cos\mu_3(x-b_3)+E_0\sin\mu_3(x-b_2)\right]\frac{\cosh\lambda_0^{(3)}(h_3-y)}{\cosh\lambda_0^{(3)}h_3}\\ +\sum_{n=1}^{\infty}\left[D_n\cosh s_n^{(3)}(x-b_3)+E_n\sinh\{s_n^{(3)}(x-b_2)\}\right]\frac{\cos\lambda_n^{(3)}(h_3-y)}{\cos\lambda_n^{(3)}h_3}, & \text{in } R_3,\\ \frac{\cosh\lambda_0^{(3)}(h_3-y)}{\cosh\lambda_0^{(3)}h_3}Te^{i\mu_3(x-b_2)}+\sum_{n=1}^{\infty}F_n\frac{\cos\lambda_n^{(3)}(h_3-y)}{\cos\lambda_n^{(3)}h_3}e^{s_n^{(3)}(x-b_2)} & \text{in } R_4;\end{cases}\tag{3.2}$$

where $\lambda_n^{(j)}$ is the wave number of evanescent mode and $\pm i\lambda_n^{(j)}(n=1,2,.....)$ satisfy the dispersion equation $\lambda(1+M\lambda^2)\tanh\lambda h_j=\frac{\omega^2}{g}$ and $s_n^{(j)}=\{(\lambda_n^{(j)})^2+\nu^2\}^{\frac{1}{2}},(j=1,2,3)$ and $\mu_2=\{(\lambda_0^{(2)})^2-\nu^2\}^{\frac{1}{2}}$.

The velocity potentials satisfy the following boundary conditions also

$$\phi_x(b_j-0,y)=\phi_x(b_j+0,y)=f_j(y),\quad 0<y<h_j\tag{3.3}$$

where $b_j=-b_1$ for $j=1$, $b_j=0$, b_2 for $j=2$, $b_j=b_3$ for $j=3$ and $f_1(y)=0$, for $h_1<y<h_2$, $f_2(y)=0$ for $a_1<y<a_2$, $f_3(y)=0$ for $h_3<y<h_2$ due to the condition(2.5). The horizontal components of velocity, near the submerged corners of the barrier has square root singularity and near the corners of a rectangular trench have one-third singularity respectively, which are given as

$$f_2(y)=O(|y-a_j|^{-\frac{1}{2}})\text{ as }y\to a_j(j=1,2),\tag{3.4}$$

$$f_j(y)=O(|y-h_j|^{-\frac{1}{3}})\text{ as }y\to h_j(j=1,3).\tag{3.5}$$

Now using the expressions of the velocity potential for four regions in equations (3.3) and applying modified inversion formula [21], we have the unknown coefficients for case-I, II as

$$1-R=\frac{-4i\lambda_0^{(1)}\cosh\lambda_0^{(1)}h_1}{\mu_1\delta_0^{(1)}}\left[\int_0^{h_1}f_1(y)\cosh\lambda_0^{(1)}(h_1-y)\,dy-\frac{M}{K}\lambda_0^{(1)}\sinh\lambda_0^{(1)}h_1f_{1y}(0)\right]\tag{3.6}$$

and

$$A_n=\frac{4\lambda_n^{(1)}\cos\lambda_n^{(1)}h_1}{s_n^{(1)}\delta_n^{(1)}}\left[\int_0^{h_1}f_1(y)\cos\lambda_n^{(1)}(h_1-y)\,dy+\frac{M}{K}\lambda_n^{(1)}\sin\lambda_n^{(1)}h_1f_{1y}(0)\right]\tag{3.7}$$

with $K = \frac{\omega^2}{g}$ and

$$\delta_0^{(j)} = \frac{2\lambda_0^{(j)} h_j (1 + M{\lambda_0^{(j)}}^2) + (1 + 3M{\lambda_0^{(j)}}^2) \sinh 2\lambda_0^{(j)} h_j}{(1 + M{\lambda_0^{(j)}}^2)},$$

$$\delta_n^{(j)} = \frac{2\lambda_n^{(j)} h_j (1 - M{\lambda_n^{(j)}}^2) + (1 - 3M{\lambda_n^{(j)}}^2) \sin 2\lambda_n^{(j)} h_j}{(1 - M{\lambda_n^{(j)}}^2)}, j = 1, 2, 3 \ (n = 1, 2, ...).$$

Moreover,

$$B_0 = \frac{8\lambda_0^{(2)} \cosh \lambda_0^{(2)} h_2}{\delta_0^{(2)} \mu_2 \sin 2\mu_2 (b_1 + b_2)} \left[\int_0^{h_1} f_1(y) \cosh \lambda_0^{(2)} (h_2 - y) dy - \frac{M}{K} \lambda_0^{(2)} \sinh \lambda_0^{(2)} h_2 \ f_{1y}(0) \right]$$
$$- \frac{4\lambda_0^{(2)} \cosh \lambda_0^{(2)} h_2}{\delta_0^{(2)} \mu_2 \sin \mu_2 (b_1 + b_2)} \left[\int_0^{h_2} f_2(y) \cosh \lambda_0^{(2)} (h_2 - y) \ dy - \frac{M}{K} \lambda_0^{(2)} \sinh \lambda_0^{(2)} h_2 \ f_{2y}(0) \right], \tag{3.8}$$

$$B_n = \frac{4\lambda_n^{(2)} \cos \lambda_n^{(2)} h_2}{\delta_n^{(2)} s_n^{(2)} \sinh s_n^{(2)} (b_1 + b_2)} \left[\int_0^{h_2} f_2(y) \cos \lambda_n^{(2)} (h_2 - y) dy + \frac{M}{K} \lambda_n^{(2)} \sin \lambda_n^{(2)} h_2 \ f_{2y}(0) \right]$$
$$- \frac{8\lambda_n^{(2)} \cos \lambda_n^{(2)} h_2}{\delta_n^{(2)} s_n^{(2)} \sinh 2s_n^{(2)} (b_1 + b_2)} \left[\int_0^{h_1} f_1(y) \cos \lambda_n^{(2)} (h_2 - y) dy + \frac{M}{K} \lambda_n^{(2)} \sin \lambda_n^{(2)} h_2 \ f_{1y}(0) \right]; \tag{3.9}$$

$$C_0 = \frac{4\lambda_0^{(2)} \cosh \lambda_0^{(2)} h_2}{\delta_0^{(2)} \mu_2 \cos \mu_2 (b_1 + b_2)} \left[\int_0^{h_1} f_1(y) \cosh \lambda_0^{(2)} (h_2 - y) dy - \frac{M}{K} \lambda_0^{(2)} \sinh \lambda_0^{(2)} h_2 \ f_{1y}(0) \right], \tag{3.10}$$

$$C_n = \frac{4\lambda_n^{(2)} \cos \lambda_n^{(2)} h_2}{\delta_n^{(2)} s_n^{(2)} \cosh s_n^{(2)} (b_1 + b_2)} \left[\int_0^{h_1} f_1(y) \cos \lambda_n^{(2)} (h_2 - y) \ dy + \frac{M}{K} \lambda_n^{(2)} \sin \lambda_n^{(2)} h_2 \ f_{1y}(0) \right]; \tag{3.11}$$

$$D_0 = \frac{8\lambda_0^{(2)} \cosh \lambda_0^{(2)} h_2}{\delta_0^{(2)} \mu_2 \sin 2\mu_2 (b_3 - b_2)} \left[\int_0^{h_2} f_2(y) \cosh \lambda_0^{(2)} (h_2 - y) dy - \frac{M}{K} \lambda_0^{(2)} \sinh \lambda_0^{(2)} h_2 \ f_{2y}(0) \right]$$
$$- \frac{4\lambda_0^{(2)} \cosh \lambda_0^{(2)} h_2}{\delta_0^{(2)} \mu_2 \sin \mu_2 (b_3 - b_2)} \left[\int_0^{h_3} f_3(y) \cosh \lambda_0^{(2)} (h_2 - y) dy - \frac{M}{K} \lambda_0^{(2)} \sinh \lambda_0^{(2)} h_2 \ f_{3y}(0) \right], \tag{3.12}$$

$$D_n = \frac{4\lambda_n^{(2)} \cos \lambda_n^{(2)} h_2}{\delta_n^{(2)} s_n^{(2)} \sinh s_n^{(2)} (b_3 - b_2)} \left[\int_0^{h_3} f_3(y) \cos \lambda_n^{(2)} (h_2 - y) dy + \frac{M}{K} \lambda_n^{(2)} \sin \lambda_n^{(2)} h_2 \ f_{3y}(0) \right]$$
$$- \frac{8\lambda_n^{(2)} \cos \lambda_n^{(2)} h_2}{\delta_n^{(2)} s_n^{(2)} \sinh 2s_n^{(2)} (b_3 - b_2)} \left[\int_0^{h_2} f_2(y) \cos \lambda_n^{(2)} (h_2 - y) dy + \frac{M}{K} \lambda_n^{(2)} \sin \lambda_n^{(2)} h_2 \ f_{2y}(0) \right]; \tag{3.13}$$

$$E_0 = \frac{4\lambda_0^{(2)} \cosh \lambda_0^{(2)} h_2}{\delta_0^{(2)} \mu_2 \cos \mu_2 (b_3 - b_2)} \left[\int_0^{h_2} f_2(y) \cosh \lambda_0^{(2)} (h_2 - y) \ dy - \frac{M}{K} \lambda_0^{(2)} \sinh \lambda_0^{(2)} h_2 \ f_{2y}(0) \right], \tag{3.14}$$

$$E_n = \frac{4\lambda_n^{(2)} \cos \lambda_n^{(2)} h_2}{\delta_n^{(2)} s_n^{(2)} \cosh s_n^{(2)} (b_3 - b_2)} \left[\int_0^{h_2} f_2(y) \cos \lambda_n^{(2)} (h_2 - y) \ dy + \frac{M}{K} \lambda_n^{(2)} \sin \lambda_n^{(2)} h_2 \ f_{2y}(0) \right]; \tag{3.15}$$

$$T = \frac{-4i\lambda_0^{(3)} \cosh \lambda_0^{(3)} h_3}{\mu_3 \delta_0^{(3)}} \left[\int_0^{h_3} f_3(y) \cosh \lambda_0^{(3)} (h_3 - y) \ dy - \frac{M}{K} \lambda_0^{(3)} \sinh \lambda_0^{(3)} h_3 \ f_{3y}(0) \right], \tag{3.16}$$

and

$$F_n = \frac{4\lambda_n^{(3)}\cos\lambda_n^{(3)}h_3}{s_n^{(3)}\delta_n^{(3)}}\bigg[\int_0^{h_3} f_3(y)\cos\lambda_n^{(3)}(h_3-y)\ dy + \frac{M}{K}\lambda_n^{(3)}\sin\lambda_0^{(3)}h_3\ f_{3y}(0)\bigg]. \tag{3.17}$$

3.1. **Reduction to integral equation.** Now the pressure continuous at $x=-b_1, y\in(0,h_1)$ $x=0,\ b_2, y\in(0,a_1)\cup(a_2,h_2)$ and $x=b_3, y\in(0,h_3)$ yields

$$\phi(-b_{1-},y)=\phi(-b_{1+},y),\ y\ \in(0,h_1), \tag{3.18}$$

$$\phi(0_-,y)=\phi(0_+,y),\ y\ \in(0,a_1)\cup(a_2,h_2), \tag{3.19}$$

$$\phi(b_{2-},y)=\phi(b_{2-},y),\ y\ \in(0,a_1)\cup(a_2,h_2), \tag{3.20}$$

$$\phi(b_{3-},y)=\phi(b_{3+},y),\ y\ \in(0,h_3). \tag{3.21}$$

These form the integral equations

$$\int_0^{h_1} F_1(u)M_1(y,u)\ du+\int_0^{h_2} F_2(u)M_2(y,u)\ du=\ \psi_1(y),\ y\in(0,h_1), \tag{3.22}$$

$$\int_0^{h_1} F_1(u)M_3(y,u)\ du+\int_0^{h_2} F_2(u)M_4(y,u)\ du+\int_0^{h_3} F_3(u)M_5(y,u)\ du=\psi_2(y),\ y\in(0,h_2), \tag{3.23}$$

$$\int_0^{h_2} F_2(u)M_6(y,u)\ du+\int_0^{h_3} F_3(u)M_7(u)(y,u)\ du=\ \psi_3(y),\ y\in(0,h_3), \tag{3.24}$$

where

$$F_i(y)=\frac{4}{(1+R)}\ f_i(y),\ i=1,2,3 \tag{3.25}$$

and $M_i(y,u),\ i=1,2,.....,7$ are real and symmetric in y and u; $\psi_i(y),\ i=1,2,3$ and their expressions are given below

$$\begin{aligned}M_1(y,u)=&\frac{2\lambda_0^{(2)}\cosh\lambda_0^{(2)}(h_2-y)\cosh\lambda_0^{(2)}(h_2-u)}{\delta_0^{(2)}\mu_2\sin 2\mu_2(b_1+b_2)}-\frac{\lambda_0^{(2)}\cosh\lambda_0^{(2)}(h_2-y)\cosh\lambda_0^{(2)}(h_2-u)}{\delta_0^{(2)}\mu_2\cot\mu_2(b_1+b_2)}\\&-\sum_{n=1}^{\infty}\bigg(\frac{2\lambda_n^{(2)}\cos\lambda_n^{(2)}(h_2-y)\cos\lambda_n^{(2)}(h_2-u)}{\delta_n^{(2)}s_n^{(2)}\sinh 2s_n^{(2)}(b_1+b_2)}+\frac{\lambda_n^{(2)}\cos\lambda_n^{(2)}(h_2-y)\cos\lambda_n^{(2)}(h_2-u)}{\delta_n^{(2)}s_n^{(2)}\coth s_n^{(2)}(b_1+b_2)}\\&+\frac{\lambda_n^{(1)}\cos\lambda_n^{(1)}(h_1-y)\cos\lambda_n^{(1)}(h_1-u)}{s_n^{(1)}\delta_n^{(1)}}\bigg),\end{aligned} \tag{3.26}$$

$$M_2(y,u)=-\frac{\lambda_0^{(2)}\cosh\lambda_0^{(2)}(h_2-y)\cosh\lambda_0^{(2)}(h_2-u)}{\delta_0^{(2)}\mu_2\sin\mu_2(b_1+b_2)}+\sum_{n=1}^{\infty}\frac{\lambda_n^{(2)}\cos\lambda_n^{(2)}(h_2-y)\cos\lambda_n^{(2)}(h_2-u)}{\delta_n^{(2)}s_n^{(2)}\sinh s_n^{(2)}(b_1+b_2)}, \tag{3.27}$$

$$M_3(y,u)=M_2(y,u), \tag{3.28}$$

$$\begin{aligned}M_4(y,u)=&\frac{\lambda_0^{(2)}\cosh\lambda_0^{(2)}(h_2-y)\cosh\lambda_0^{(2)}(h_2-u)}{\delta_0^{(2)}\mu_2\tan\mu_2(b_1+b_2)}+\frac{2\lambda_0^{(2)}\cosh\lambda_0^{(2)}(h_2-y)\cosh\lambda_0^{(2)}(h_2-u)}{\delta_0^{(2)}\mu_2\sin 2\mu_2(b_3-b_2)}\\&-\frac{\lambda_0^{(2)}\cosh\lambda_0^{(2)}(h_2-y)\cosh\lambda_0^{(2)}(h_2-u)}{\delta_0^{(2)}\mu_2\cot\mu_2(b_3-b_2)}-\sum_{n=1}^{\infty}\bigg(\frac{\lambda_n^{(2)}\cos\lambda_n^{(2)}(h_2-y)\cos\lambda_n^{(2)}(h_2-u)}{\delta_n^{(2)}s_n^{(2)}\tanh s_n^{(2)}(b_1+b_2)}\\&+\frac{2\lambda_n^{(2)}\cos\lambda_n^{(2)}(h_2-y)\cos\lambda_n^{(2)}(h_2-u)}{\delta_n^{(2)}s_n^{(2)}\sinh 2s_n^{(2)}(b_3-b_2)}+\frac{\lambda_n^{(2)}\cos\lambda_n^{(2)}(h_2-y)\cos\lambda_n^{(2)}(h_2-u)}{\delta_n^{(2)}s_n^{(2)}\coth s_n^{(2)}(b_3-b_2)}\bigg),\end{aligned} \tag{3.29}$$

$$M_5(y,u) = -\frac{\lambda_0^{(2)}\cosh\lambda_0^{(2)}(h_2-y)\cosh\lambda_0^{(2)}(h_2-u)}{\delta_0^{(2)}\mu_2\sin\mu_2(b_3-b_2)} + \sum_{n=1}^{\infty}\frac{\lambda_n^{(2)}\cos\lambda_n^{(2)}(h_2-y)\cos\lambda_n^{(2)}(h_2-u)}{\delta_n^{(2)}s_n^{(2)}\sinh s_n^{(2)}(b_3-b_2)}, \tag{3.30}$$

$$M_6(y,u) = M_5(y,u), \tag{3.31}$$

$$M_7(y,u) = \frac{\lambda_0^{(2)}\cosh\lambda_0^{(2)}(h_2-y)\cosh\lambda_0^{(2)}(h_2-u)}{\delta_n^{(2)}\mu_2\tan\mu_2(b_3-b_2)} - \frac{i\lambda_0^{(3)}\cosh\lambda_0^{(3)}(h_3-y)\cosh\lambda_0^{(3)}(h_3-u)}{\delta_0^{(3)}\mu_3} - \sum_{n=1}^{\infty}\left(\frac{\lambda_n^{(2)}\cos\lambda_n^{(2)}(h_2-y)\cos\lambda_n^{(2)}(h_2-u)}{\delta_n^{(2)}s_n^{(2)}\tanh s_n^{(2)}(b_3-b_2)} - \frac{\lambda_n^{(3)}\cos\lambda_n^{(3)}(h_3-y)\cos\lambda_n^{(3)}(h_3-u)}{\delta_n^{(3)}s_n^{(3)}}\right), \tag{3.32}$$

$$\begin{aligned}\psi_1 = {} & \left[\frac{-2f_{1y}(0)}{\sin 2\mu_2(b_1+b_2)} + \frac{f_{2y}(0)}{\sin\mu_2(b_1+b_2)} + \frac{f_{1y}(0)}{\cot\mu_2(b_1+b_2)}\right]\frac{M\{\lambda_0^{(2)}\}^2\sinh\lambda_0^{(2)}h_2\cosh\lambda_0^{(2)}(h_2-y)}{\mu_2\delta_0^{(2)}K} \\ & - \sum_{n=1}^{\infty}\left[\frac{2f_{1y}(0)}{\sinh 2s_n^{(2)}(b_1+b_2)} - \frac{f_{2y}(0)}{\sinh s_n^{(2)}(b_1+b_2)} + \frac{f_{1y}(0)}{\coth s_n^{(2)}(b_1+b_2)}\right]\cdot \\ & \qquad \frac{M\{\lambda_n^{(2)}\}^2\sin\lambda_n^{(2)}h_2\cos\lambda_n^{(2)}(h_2-y)}{\delta_n^{(2)}s_n^{(2)}K} \\ & + \frac{\cosh\lambda_0^{(1)}(h_1-y)}{\cosh\lambda_0^{(1)}h_1} + \frac{M\{\lambda_n^{(1)}\}^2\sin\lambda_n^{(1)}h_1\ f_{1y}(0)}{s_n^{(1)}\delta_n^{(1)}K}\cos\lambda_n^{(1)}(h_1-y),\end{aligned} \tag{3.33}$$

$$\begin{aligned}\psi_2 = {} & \left[\frac{f_{1y}(0)}{\sin\mu_2(b_1+b_2)} - \frac{f_{2y}(0)}{\tan\mu_2(b_1+b_2)} - \frac{2f_{2y}(0)}{\sin 2\mu_2(b_3-b_2)} + \frac{f_{3y}(0)}{\sin\mu_2(b_3-b_2)} - \frac{f_{2y}(0)}{\cot\mu_2(b_3-b_2)}\right]* \\ & \frac{M\{\lambda_0^{(2)}\}^2\sinh\lambda_0^{(2)}h_2\cosh\lambda_0^{(2)}(h_2-y)}{\mu_2\delta_0^{(2)}K} \\ & + \sum_{n=1}^{\infty}\left[\frac{f_{2y}(0)}{\sinh s_n^{(2)}(b_1+b_2)} - \frac{f_{1y}(0)}{\tanh s_n^{(2)}(b_1+b_2)} + \frac{f_{3y}(0)}{\sinh s_n^{(2)}(b_3-b_2)}\right. \\ & \left. - \frac{2f_{2y}(0)}{\sinh 2s_n^{(2)}(b_3-b_2)} - \frac{f_{2y}(0)}{\coth s_n^{(2)}(b_3-b_2)}\right]\frac{M\{\lambda_n^{(2)}\}^2\sin\lambda_n^{(2)}h_2\cos\lambda_n^{(2)}(h_2-y)}{\delta_n^{(2)}s_n^{(2)}K},\end{aligned} \tag{3.34}$$

$$\begin{aligned}\psi_3 = {} & \left[-\frac{f_{2y}(0)}{\sin\mu_2(b_3-b_2)} + \frac{f_{3y}(0)}{\tan\mu_2(b_3-b_2)}\right]\frac{M\{\lambda_0^{(2)}\}^2\sinh\lambda_0^{(2)}h_2\cosh\lambda_0^{(2)}(h_2-y)}{\delta_0^{(2)}\mu_2K} \\ & + \sum_{n=1}^{\infty}\left[\frac{f_{2y}(0)}{\sinh s_n^{(2)}(b_3-b_2)} - \frac{f_{3y}(0)}{\tanh s_n^{(2)}(b_3-b_2)}\right]\frac{M\{\lambda_n^{(2)}\}^2\sin\lambda_n^{(2)}h_2\cos\lambda_n^{(2)}(h_2-y)}{\delta_n^{(2)}s_n^{(2)}K} \\ & + \frac{iM\{\lambda_0^{(3)}\}^2\sinh\lambda_0^{(3)}h_3\ f_{3y}(0)}{\mu_3\delta_0^{(3)}K}\cosh\lambda_0^{(3)}(h_3-y) \\ & + \sum_{n=1}^{\infty}\frac{M\{\lambda_n^{(3)}\}^2\sin\lambda_n^{(3)}h_3\ f_{3y}(0)}{s_n^{(3)}\delta_n^{(3)}K}\cos\lambda_n^{(3)}(h_3-y).\end{aligned} \tag{3.35}$$

Here we get three integral equations (3.22)-(3.24) in different ranges, they can be extended as in Roy et al [29] and combined together by multiplying with appropriate basis functions of suitable weights.

3.2. **Solution of the integral equation using two numerical methods.**

3.2.1. *Boundary element method.* Since the unknown functions of the Integral equations, (3.22)-(3.24) i.e., $F_1(y), F_2(y), F_3(y)$ have one-third, half, one-third singularities at $x = -b_1; 0, b_2; b_3$ as relation (2.7)-(2.8), so construct

$$F_1(y) = \sqrt[3]{(h_1 - y)}\mathcal{F}_1(y), \tag{3.36}$$

$$F_2(y) = \sqrt{(a_1 - y)(y - a_2)}\mathcal{F}_2(y), \tag{3.37}$$

and

$$F_3(y) = \sqrt[3]{(h_3 - y)}\mathcal{F}_3(y) \tag{3.38}$$

where$\mathcal{F}_1(y), \mathcal{F}_2(y), \mathcal{F}_3(y)$ are a regular function in $y \in [0, h_1], y \in (0, a_1) \cup (a_2, h_2), y \in [0, h_3]$ respectively.

Substituting (3.36)-(3.38) in equations (3.22)-(3.24), we reconstruct the I.E. as

$$\int_0^{h_1} \mathcal{F}_1(u)\mathcal{M}_1(y,u)\ du + \int_0^{h_2} \mathcal{F}_2(u)\mathcal{M}_2(y,u)\ du = \psi_1(y) \tag{3.39}$$

$$\int_0^{h_1} \mathcal{F}_1(u)\mathcal{M}_3(y,u)\ du + \int_0^{h_2} \mathcal{F}_2(u)\mathcal{M}_4(y,u)\ du + \int_0^{h_3} \mathcal{F}_3(u)\mathcal{M}_5(y,u)\ du = \psi_2(y) \tag{3.40}$$

$$\int_0^{h_2} \mathcal{F}_2(u)\mathcal{M}_6(y,u)\ du + \int_0^{h_3} \mathcal{F}_3(u)\mathcal{M}_7(u)(y,u)\ du = \psi_3(y) \tag{3.41}$$

where

$$\begin{cases} \mathcal{M}_1(y,u) = \sqrt[3]{(h_1 - y)}M_1(y,u), \\ \mathcal{M}_2(y,u) = \sqrt{(a_1 - y)(y - a_2)}M_2(y,u), \\ \mathcal{M}_3(y,u) = \sqrt[3]{(h_1 - y)}M_3(y,u), \\ \mathcal{M}_4(y,u) = \sqrt{(a_1 - y)(y - a_2)}M_4(y,u), \\ \mathcal{M}_5(y,u) = \sqrt[3]{(h_3 - y)}M_5(y,u) \\ \mathcal{M}_6(y,u) = \sqrt{(a_1 - y)(y - a_2)}M_6(y,u), \\ \mathcal{M}_7(y,u) = \sqrt[3]{(h_3 - y)}M_7(y,u) \end{cases} \tag{3.42}$$

We divide the first interval $[0, h_1]$ into n_1 number of subintervals and the subintervals are such that $[0, h_1] = \bigcup_{i=0}^{n_1}[a_{i-1}, a_i]$ and devide the second interval $[0, h_2]$ into n_2 number of subintervals such that $[0, h_2] = \bigcup_{j=0}^{n_2}[b_{j-1}, b_j]$ and again devide the third interval $[0, h_3]$ into n_3 number of subintervals such that $[0, h_3] = \bigcup_{k=0}^{n_3}[c_{k-1}, c_k]$ with $a_0 = 0; a_i = a_0 + ir_1$; $b_0 = 0; b_j = b_0 + jr_2$ and $c_0 = 0; c_k = c_0 + kr_3$; where $r_1 = \frac{h_1 - 0}{n_1}$, $r_2 = \frac{h_2 - 0}{n_2}$, $r_3 = \frac{h_3 - 0}{n_3}$.

Now we take $u = u1_i \in [a_{i-1}, a_i], i = 1, 2, ..., n_1, u = u2_i \in [b_{j-1}, a_j], j = 1, 2, ..., n_2, u = u3_i \in [c_{k-1}, c_k], k = 1, 2, ..., n_3$ so,

$$\begin{cases} u1_i = (1 - \xi)a_{i-1} + \xi a_i, \\ u2_j = (1 - \xi)b_{j-1} + \xi b_j \qquad 0 \le \xi \le 1 \\ u3_k = (1 - \xi)c_{k-1} + \xi c_k \end{cases} \tag{3.43}$$

Also, when y belongs to the line element $[a_{i-1}, a_i], i = 1, 2, , n_1$, we write, $y = y1_i = (1 - \eta)a_{i-1} + \eta a_i$, when y belongs to the line element $[b_{j-1}, b_j], j = 1, 2, , n_2$, we write, $y = y2_j = (1 - \eta)b_{j-1} + \eta b_j, 0 \le$

$\eta \leq 1$. Again, similarly when y belongs to the line element $[c_{k-1}, c_k], k = 1, 2, , n_3$, we write, $y = y3_k = (1-\zeta)c_{k-1} + \zeta c_k, 0 \leq \zeta \leq 1$. So (3.22)-(3.24) can be written as

$$\begin{cases} \sum_{i=1}^{n_1} \int_0^1 \mathcal{F}_1(u1_i)\mathcal{M}(y1_p, u1_i)r_1 d\xi + \sum_{j=1}^{n_2} \int_0^1 \mathcal{F}_2(u2_j)\mathcal{M}(y1_p, u2_j)r_2 d\xi = \psi_1(y1_p), \\ p = 1, 2, ..., n_1, \\ \sum_{i=1}^{n_1} \int_0^1 \mathcal{F}_1(u1_i)\mathcal{M}(y2_q, u1_i)r_1 d\xi + \sum_{j=1}^{n_2} \int_0^1 \mathcal{F}_2(u2_j)\mathcal{M}(y2_q, u2_j)r_2 d\xi = \psi_1(y2_q), \\ q = 1, 2, ..., n_2; \end{cases} \tag{3.44}$$

$$\begin{cases} \sum_{i=1}^{n_1} \int_0^1 \mathcal{F}_1(u1_i)\mathcal{M}(y1_p, u1_i)r_1 d\xi + \sum_{j=1}^{n_2} \int_0^1 \mathcal{F}_2(u2_j)\mathcal{M}(y1_p, u2_j)r_2 d\xi \\ \qquad + \sum_{k=1}^{n_3} \int_0^1 \mathcal{F}_3(u3_k)\mathcal{M}(y1_p, u3_k)r_3 d\xi = \psi_2(y1_p), \ p = 1, 2, ..., n_1, \\ \sum_{i=1}^{n_1} \int_0^1 \mathcal{F}_1(u1_i)\mathcal{M}(y2_q, u1_i)r_1 d\xi + \sum_{j=1}^{n_2} \int_0^1 \mathcal{F}_2(u2_j)\mathcal{M}(y2_q, u2_j)r_2 d\xi \\ \qquad + \sum_{k=1}^{n_3} \int_0^1 \mathcal{F}_3(u3_k)\mathcal{M}(y2_q, u3_k)r_3 d\xi = \psi_2(y2_q), \ q = 1, 2, ..., n_2, \\ \sum_{i=1}^{n_1} \int_0^1 \mathcal{F}_1(u1_i)\mathcal{M}(y3_r, u1_i)r_1 d\xi + \sum_{j=1}^{n_2} \int_0^1 \mathcal{F}_2(u2_j)\mathcal{M}(y3_r, u2_j)r_2 d\xi \\ \qquad + \sum_{k=1}^{n_3} \int_0^1 \mathcal{F}_3(u3_k)\mathcal{M}(y3_r, u3_k)r_3 d\xi = \psi_2(y3_r), \ r = 1, 2, ..., n_3; \end{cases} \tag{3.45}$$

$$\begin{cases} \sum_{j=1}^{n_2} \int_0^1 \mathcal{F}_2(u2_j)\mathcal{M}(y2_q, u2_j)r_2 d\xi + \sum_{k=1}^{n_3} \int_0^1 \mathcal{F}_3(u3_k)\mathcal{M}(y2_q, u3_k)r_3 d\xi = \psi_3(y2_q), \\ q = 1, 2, ..., n_2, \\ \sum_{j=1}^{n_2} \int_0^1 \mathcal{F}_2(u2_j)\mathcal{M}(y3_r, u2_j)r_2 d\xi + \sum_{k=1}^{n_3} \int_0^1 \mathcal{F}_3(u3_k)\mathcal{M}(y3_r, u3_k)r_3 d\xi = \psi_3(y3_r), \\ r = 1, 2, ..., n_3. \end{cases} \tag{3.46}$$

Now in boundary element method we take the consideration that the unknown function of the integral equation takes constant values in each small subintervals. So assume $\mathcal{F}_1(u1_i) = \mathcal{F}_1(i) =$ constant where $u1_i \in [a_{i-1}, a_i], i = 1, 2, ..., n_1$, $\mathcal{F}_2(u2_j) = \mathcal{F}_2(j) =$ constant where $u2_j \in [b_{j-1}, b_j], j = 1, 2, ..., n_2$ and $\mathcal{F}_3(u3_k) = \mathcal{F}_3(k) =$ constant where $u3_k \in [c_{k-1}, c_k], k = 1, 2, ..., n_3$. So under this approximation, integral equations (3.44)-(3.46) reduces to a system of linear equation written as

$$\sum_{i=1}^{n_1} \mathcal{F}_1(i) \begin{Bmatrix} \mathcal{M}(p,i) \\ \mathcal{M}(q,i) \end{Bmatrix} + \sum_{j=1}^{n_2} \mathcal{F}_2(j) \begin{Bmatrix} \mathcal{M}(p,j) \\ \mathcal{M}(q,j) \end{Bmatrix} = \begin{Bmatrix} \psi_1(p) \\ \psi_1(q) \end{Bmatrix}, \tag{3.47}$$

$$\sum_{i=1}^{n_1} \mathcal{F}_1(i) \begin{Bmatrix} \mathcal{M}(p,i) \\ \mathcal{M}(q,i) \\ \mathcal{M}(r,i) \end{Bmatrix} + \sum_{j=1}^{n_2} \mathcal{F}_2(j) \begin{Bmatrix} \mathcal{M}(p,j) \\ \mathcal{M}(q,j) \\ \mathcal{M}(r,j) \end{Bmatrix} + \sum_{k=1}^{n_3} \mathcal{F}_3(k) \begin{Bmatrix} \mathcal{M}(p,k) \\ \mathcal{M}(q,k) \\ \mathcal{M}(r,k) \end{Bmatrix} = \begin{Bmatrix} \psi_2(p) \\ \psi_2(q) \\ \psi_2(r) \end{Bmatrix}, \tag{3.48}$$

$$\sum_{j=1}^{n_2} \mathcal{F}_2(j) \begin{Bmatrix} \mathcal{M}(q,j) \\ \mathcal{M}(r,j) \end{Bmatrix} + \sum_{k=1}^{n_3} \mathcal{F}_3(k) \begin{Bmatrix} \mathcal{M}(q,k) \\ \mathcal{M}(r,k) \end{Bmatrix} = \begin{Bmatrix} \psi_3(q) \\ \psi_3(r) \end{Bmatrix} \tag{3.49}$$

where

$$\begin{cases} \mathcal{M}(p,i) = \int_0^1 \mathcal{M}(y1_p, u1_i)r_1 d\xi, \mathcal{M}(p,j) = \int_0^1 \mathcal{M}(y1_p, u2_j)r_2 d\xi, \mathcal{M}(p,k) = \int_0^1 \mathcal{M}(y1_p, u3_k)r_3 d\xi \\ \mathcal{M}(q,i) = \int_0^1 \mathcal{M}(y2_q, u1_i)r_1 d\xi, \mathcal{M}(q,j) = \int_0^1 \mathcal{M}(y2_q, u2_j)r_2 d\xi, \mathcal{M}(q,k) = \int_0^1 \mathcal{M}(y2_q, u3_k)r_3 d\xi \\ \mathcal{M}(r,i) = \int_0^1 \mathcal{M}(y3_r, u1_i)r_1 d\xi, \mathcal{M}(r,j) = \int_0^1 \mathcal{M}(y3_r, u2_j)r_2 d\xi, \mathcal{M}(r,k) = \int_0^1 \mathcal{M}(y3_r, u3_k)r_3 d\xi, \\ \psi_1(p) = \psi_1(y1_p), \ \psi_1(q) = \psi_1(y2_q), \ \psi_2(p) = \psi_2(y1_p), \ \psi_2(q) = \psi_2(y2_q), \ \psi_2(r) = \psi_(y3_r), \\ \psi_3(q) = \psi_3(y2_q), \ \psi_3(r) = \psi_3(y3_r). \end{cases} \tag{3.50}$$

Solving the system of equation (3.48)-(3.50) , we obtain the unknown constants $\mathcal{F}_1(i)$, for $i = 1, 2, ..., n_1$, $\mathcal{F}_2(j)$, for $j = 1, 2, ..., n_2$ and $\mathcal{F}_3(k)$, for $k = 1, 2, ..., n_3$. Hence $|R|, |T|$ can be evaluated from equations (3.6) and (3.25) as

$$R = \frac{1+\Omega}{1-\Omega} \tag{3.51}$$

where

$$\Omega = \frac{4i\lambda_0^{(1)}\cosh\lambda_0^{(1)}h_1}{\mu_1\delta_0^{(1)}}\sum_{n=i}^{n_1}\mathcal{F}_1(i)\int_0^1\cosh\lambda_0^{(1)}(h_1-y1_i)\ r_1 d\xi \tag{3.52}$$

and

$$T = -\frac{4i(1+R)\lambda_0^{(3)}\cosh\lambda_0^{(3)}h_3}{\mu_3\delta_0^{(3)}}\sum_{n=k}^{n_3}\mathcal{F}_3(k)\int_0^1\cosh\lambda_0^{(3)}(h_3-y3_k)\ r_3 d\xi. \tag{3.53}$$

3.2.2. *Multiterm Galerkin method.* To solve the integral equations (3.22)-(3.24), we employ the multi-term Galerkin Approximation method. The unknown functions $F_i(y),\ i=1,2,3$ are approximated as

$$F_1(y) \approx \mathcal{F}_1(y), 0<y<h_1, \tag{3.54}$$

$$F_2(y) \approx \mathcal{F}_2(y), 0<y<h_2, \tag{3.55}$$

$$F_3(y) \approx \mathcal{F}_3(y), 0<y<h_3, \tag{3.56}$$

where $\mathcal{F}_i(y),\ i=1,2,3$ have multi-term Galerkin expansions in terms of suitable basis functions given by

$$\mathcal{F}_1(y) = \sum_{n=0}^{N} a_n\ p_n(y), \tag{3.57}$$

$$\mathcal{F}_2(y) = \sum_{n=0}^{N} b_n\ q_n(y), \tag{3.58}$$

$$\mathcal{F}_3(y) = \sum_{n=0}^{N} c_n\ r_n(y), \tag{3.59}$$

with unknown constants a_n, b_n, c_n where the basis functions $p_n(y)$ for $0<y<h_1$, $r_n(y)$ for $0<y<h_3$, $q_n(y)$ for $0<y<a_1$, $a_1<y<a_2$ and $a_2<y<h_2$, are chosen in terms of ultraspherical Gegenbauer polynomial of order $\frac{1}{6}$ and Chebychev polynomials respectively. The basis functions in various intervals are given below.

Choice of Basis Functions

Case-I:

Since the horizontal component of velocity near points $(-b_1, h_1)$ of the trench has a cube-root singularity [12], the basis function $p_m(y)$ as

$$p_m(y) = -\frac{d}{dy}\left[e^{-Ky}\int_y^{h_1} e^{Kt}\hat{p_m}(t)\ dt\right],\quad 0<y<h_1 \tag{3.60}$$

with

$$\hat{p_m}(y) = \frac{2^{\frac{7}{6}}\Gamma(\frac{1}{6})(2m)!}{\pi\Gamma(2m+\frac{1}{3})h_1^{\frac{1}{3}}\{h_1^2-y^2\}^{\frac{1}{3}}}\ C_{2m}^{\frac{1}{6}}\left(\frac{y}{h_1}\right),\ 0<y<h_1. \tag{3.61}$$

Due to the square-root singularity [27] at the surrounding of the sharp submerged edges of the rigid barrier, we choose the basis function $q_m(y)$ as

$$q_m(y) \;=\; -\frac{d}{dy}\left[e^{-Ky}\int_y^{h_2} e^{Kt}\hat{q_m}(t)\;dt\right],\quad 0<y<h_2 \tag{3.62}$$

with

$$q_m(y) \;=\; \begin{cases} \frac{2(-1)^m}{\pi(a_1^2-y^2)^{\frac{1}{2}}}\;T_{2m}\left(\frac{y}{a_1}\right),\; 0<y<a_1, \\ \frac{2\{(y-a_1)(a_2-y)\}^{\frac{1}{2}}}{\pi(n+1)(a_2-a_1)h_2}\;U_m\left(\frac{2y-a_1-a_2}{a_2-a_1}\right),\; a_1<y<a_2, \\ \frac{2(-1)^m}{\pi\{(h_2-a_2)^2-(h_2-y^2)\}^{\frac{1}{2}}}\;T_{2m}\left(\frac{h_2-y}{h_2-a_2}\right),\; a_2<y<h_2. \end{cases} \tag{3.63}$$

Since the horizontal component of velocity near points (b_3, h_3) of the trench has a cube-root singularity [12], the basis function $r_m(y)$ as

$$r_m(y) \;=\; -\frac{d}{dy}\left[e^{-Ky}\int_y^{h_3} e^{Kt}\hat{r_m}(t)\;dt\right],\quad 0<y<h_3 \tag{3.64}$$

with

$$\hat{r_m}(y) = \frac{2^{\frac{7}{6}}\Gamma(\frac{1}{6})(2m)!}{\pi\Gamma(2m+\frac{1}{3})h_3^{\frac{1}{3}}\{h_3^2-y^2\}^{\frac{1}{3}}}\;C_{2m}^{\frac{1}{6}}\left(\frac{y}{h_3}\right),\; 0<y<h_3. \tag{3.65}$$

We substitute the approximations (3.57), (3.58) and (3.59) in equations (3.22)-(3.24) respectively, and then multiplying with appropriate basis functions which are already mentioned above and integrate over different ranges to obtain the linear system of equations. Solving the linear systems, we obtain the constants $a_n, b_n, c_n, n = 0, 1, 2, ..., N$ and then the relations (3.6) and (3.25) produce

$$R \;=\; \frac{1+w}{1-w} \tag{3.66}$$

where

$$w \;=\; \frac{4i\lambda_0^{(1)}\cosh\lambda_0^{(1)}h_1}{\mu_1\delta_0^{(1)}}\;\sum_{n=0}^{N} a_n\int_0^{h_1} p_n(y)\;\cosh\lambda_0^{(1)}(h_1-y)\;dy \tag{3.67}$$

and

$$T \;=\; -\frac{4i(1+R)\lambda_0^{(3)}\cosh\lambda_0^{(3)}h_3}{\mu_3\delta_0^{(3)}}\;\sum_{n=0}^{N} c_n\int_0^{h_3} r_n(y)\;\cosh\lambda_0^{(3)}(h_3-y)\;dy. \tag{3.68}$$

Case-II:

Here, numerical solutions of the integral equations (3.22)-(3.24) are obtained by using Galerkin approximation in terms of simple polynomials multiplied by a weight function by the edge condition (3.4)-(3.5). We can write $F_i(y)(i = 1, 2, 3)$ in the integral equations (3.22)-(3.24) as

$$F_1(y) = \left(\frac{h_1}{h_1-y}\right)^{\frac{1}{3}}\sum_{n=0}^{N} a_n\left(\frac{y}{h_1}\right)^n,\; 0<y<h_1, \tag{3.69}$$

$$F_2(y)=\sum_{n=0}^{N}b_n\begin{cases}\left(\frac{a_1}{a_1-y}\right)^{\frac{1}{2}}\left(\frac{y}{a_1}\right)^n, & 0<y<a_1\\ \sqrt{\frac{a_1a_2}{(y-a_1)(a_2-y)}}\left(\frac{y}{a_1}\right)^n, & a_1<y<a_2\\ \left(\frac{a_2}{y-a_2}\right)^{\frac{1}{2}}\left(\frac{y}{a_2}\right)^n, & a_2<y<h_2\end{cases}, \quad 0<y<h_2, \tag{3.70}$$

$$F_3(y)=\left(\frac{h_3}{h_3-y}\right)^{\frac{1}{3}}\sum_{n=0}^{N}c_n\left(\frac{y}{h_3}\right)^n, \ 0<y<h_3. \tag{3.71}$$

We substitute the approximations (3.69), (3.70) and (3.71) in equations (3.22)-(3.24) respectively, and then multiplying with appropriate basis functions which are already mentioned above and integrate over different ranges to obtain the linear system of equations. Solving the linear systems, we obtain

$$R \ = \ \frac{1+w_1}{1-w_1} \tag{3.72}$$

where

$$w_1 \ = \ \frac{4i\lambda_0^{(1)}\cosh\lambda_0^{(1)}h_1}{\mu_1\delta_0^{(1)}}\ \sum_{n=0}^{N}\ a_n\int_0^{h_1}\ \left(\frac{h_1}{h_1-y}\right)^{\frac{1}{3}}\left(\frac{y}{h_1}\right)^n\ \cosh\lambda_0^{(1)}(h_1-y)\ dy \tag{3.73}$$

and

$$T \ = \ -\frac{4i(1+R)\lambda_0^{(3)}\cosh\lambda_0^{(3)}h_3}{\mu_3\delta_0^{(3)}}\ \sum_{n=0}^{N}\ c_n\int_0^{h_3}\ \left(\frac{h_3}{h_3-y}\right)^{\frac{1}{3}}\left(\frac{y}{h_3}\right)^n\ \cosh\lambda_0^{(3)}(h_3-y)\ dy. \tag{3.74}$$

3.3. **Energy Balance Relation.** In this section , the energy balance relation is delivered for the present model. Considering Green's integral theorem to the function $\phi(x,y)$ and its complex conjugate $\overline{\phi}(x,y)$ in the fluid domain surrounded by the lines $y=0,-X\le x\le X;\ x=-X,0\le y\le h_1;\ y=h_1,-X\le x\le -b_1;\ x=-b_1,h_1\le y\le h_2;\ y=h_2,-b_1\le x\le b_3;\ x=b_3,h_3\le y\le h_2;\ y=h_3,b_3\le x\le X;\ x=X,0\le y\le h_3$ and $y=0,a_1\le x\le a_2$ and making ultimately $X\to\infty$. There is zero contribution from the line $y=0\ (-X\le x\le X)$ due to the upper surface boundary condition and the lines $y=h_1\ (-X\le x\le -b_1),\ y=h_2\ (-b_1\le x\le b_3),\ y=h_3\ (b_3\le x\le X)$ have no contribution because of the respective bottom conditions. Also on the lines, $y=0\ (-X\le x\le X)$ due to the upper surface boundary condition and the lines $x=-b_1\ (h_1\le y\le h_2),\ x=b_3\ (h_3\le y\le h_2)$ have zero contribution due to the given boundary condition. The contribution from the line $x=-X\ (0\le y\le h_1)$ is

$$-\frac{\mu_1\delta_0^{(1)}}{4\lambda_0^{(1)}\cosh^2\lambda_0^{(1)}h_1}(1+|R|^2) \tag{3.75}$$

and the contribution from the line $x=X\ (0\le y\le h_3)$ is

$$-\frac{\mu_3\delta_0^{(3)}}{4\lambda_0^{(3)}\cosh^2\lambda_0^{(3)}h_3}|T|^2. \tag{3.76}$$

Lastly no contribution from $x=\pm 0\ (a_1\le y\le a_2)$. After combining all these results, the Green's integral theorem produces

$$|R|^2+\mathcal{J}|T|^2=1 \tag{3.77}$$

where

$$\mathcal{J}=\frac{\mu_3\lambda_0^{(1)}\delta_0^{(3)}\cosh^2\lambda_0^{(1)}h_1}{\mu_1\lambda_0^{(3)}\delta_0^{(1)}\cosh^2\lambda_0^{(3)}h_3}. \tag{3.78}$$

This is our energy balance relation for the current model.

3.4. **Wave load.** Using the linear Bernoulli's equation, the horizontal wave force F acting on the porous barriers are obtained by integrating the dynamic pressure jumps across the barrier as

$$F = i\rho\omega \int_{a_1}^{a_2} [\phi(b_2 + 0, y) - \phi(b_2 - 0, y)]\, dy \tag{3.79}$$

where ρ is the fluid density. The non-dimensional wave load is given by

$$W_l = \frac{|F|}{F_0} \tag{3.80}$$

with

$$F_0 = \frac{\rho g\omega\{\sinh\lambda_0^{(1)}(h_2 - h_1) + \sinh\lambda_0^{(1)}h_1\}}{\lambda_0^{(1)}\cosh\lambda_0^{(1)}h_1} \tag{3.81}$$

where F_0 is the wave load acting per-unit width on a vertical rigid plate extending throughout the fluid region.

Similarly, reflection and transmission coefficients and wave load can be obtained for case-III where the thin barrier is moved right from the position $x = 0$ outside of the trench.

4. Numerical results

4.1. **Validation of the results.** In this section, we will discuss about the reflection coefficient $|R|$ and transmission coefficient $|T|$ computed numerically by solving the integral equation using Boundary element method (BEM) and multiterm Galerkin method for different values of non-dimensional parameters. Here, $|R|$ and $|T|$ are obtained numerically for different values of wave number by taking $N = 4$ in the N-term Galerkin approximations. The values of these infinite series need to be estimated by truncating r. However, the accuracy of these infinite series can be increased based on asymptotic behaviors of the Bessel function [27]. The values of $|R|$ obtained from above mentioned two methods are shown in TABLE 1 and TABLE 2 for different values of parameters. The tables show that the results by two methods agree with each other quite well.

Table 1. Reflection coefficient for $a_1/h_2 = 0.1, a_2/h_2 = 0.4, h_1/h_2 = 0.7, b_1/h_2 = 1.25, b_3/h_2 = 1.75, h_3/h_2 = 0.6, \theta = \frac{\pi}{4}, M/h_2^2 = 1.5$.

Kh_2	BEM	$Galerkin\ Method$
0.5	0.193763	0.193764
1.0	0.110917	0.110915
1.5	0.146163	0.146163
2.0	0.24697	0.24697

TABLE 3 displays $|R|$ for the fully submerged barrier at the position $x = 0$ of the trench with set of values which is given in TABLE 3 for different values of Kh_2. The numerical values computed here for N =1, 2, 3, 4, 5 and using the $(N + 1)$- term Galerkin approximations and it is seen that the results

TABLE 2. Reflection coefficient for $a_1/h_2 = 0.15, a_2/h_2 = 0.45, h_1/h_2 = 0.65, b_1/h_2 = 0.75, b_3/h_2 = 1.25, h_3/h_2 = 0.55, \theta = \frac{\pi}{4}, M/h_2^2 = 1.0$.

Kh_2	BEM	$Galerkin\ Method$
0.5	0.205393	0.205392
1.0	0.14339	0.14339
1.5	0.017991	0.017992
2.0	0.092863	0.092861

TABLE 3. Reflection coefficient for $a_1/h_2 = 0.2, a_2/h_2 = 0.5, h_1/h_2 = 0.65, b_1/h_2 = 0.5, b_3/h_2 = 0.75, h_3/h_2 = 0.55, \theta = \frac{\pi}{4}, M/h_2^2 = 1.5$.

Kh_2	$N=1$	$N=2$	$N=3$	$N=4$	$N=5$
1.0	0.11937	0.126676	0.126155	0.126205	0.126216
1.25	0.076393	0.087405	0.084569	0.085145	0.08511
1.5	0.031586	0.045565	0.044267	0.044254	0.044267
1.75	0.051586	0.053129	0.053157	0.053146	0.053179
2.0	0.092264	0.093352	0.091063	0.091265	0.091276

coincide upto 4 to 5 decimal places. It is observed from the table that the results for $|R|$ converge rapidly with N and it achieved an accuracy of three decimal places. Thus, the present procedure for the numerical computations of $|R|$ is quite efficient.

TABLE 4. Comparison results with the result of Kirby and Dalrymple for $h_2/h_1 = 3.0, b_1/h_1 = 5.0, b_3/h_1 = 5.0, h_3/h_1 = 1.0, \theta = 0, M/h_2^2 = 0$.

Kirby and Dalrymple		Present method			
		Orthogonal polynomial		Simple polynomial	
Kh_1	$\|R\|$	$\|T\|$	$\|R\|(N=5)$	$\|T\|(N=5)$	$\|R\|(N=10)$	$\|T\|(N=10)$
0.341	0.4590	0.8881	0.45903	0.88812	0.459055	0.88840
0.723	0.2960	0.9552	0.296031	0.955178	0.296021	0.955181
1.296	0.0306	0.9995	0.030614	0.999531	0.030612	0.999531

A comparative analysis of the numerical results are established in TABLE 4, by contrasting our present result with [16], considering parametric values $h_2/h_1 = 3.0, b_1/h_1 = 5.0, b_3/h_1 = 5.0, h_3/h_1 = 1.0, \theta = 0, M/h_2^2 = 0$ where the barrier is placed at the middle of the trench. We used two different types of polynomial as a basis function in Galerkin method, such as orthogonal polynomials (Gegenbauer polynomial for $\frac{1}{3}$ rd singularity and Chebyshev polynomial for half singularity) are considered as

a basis function in the method and simple polynomials are also chosen as a basis function. The rate of convergence in Galerkin method depends on the number of terms $(N+1)$ considered, from TABLE 4, one clearly observed that $N=5$ is taken in the present study for orthogonal polynomials whereas we consider $N=10$ for simple polynomials to get desired results. One can come with the conclusion that the rate of convergence with algebraic polynomials in Galerkin technique is slower than the orthogonal polynomials.

4.2. **Case-I: The barrier at middle of the trench.** When the barrier is at the position $x=0$ of the trench, numerical estimates for $|R|$ and $|T|$ are evaluated for different values of parameters $a_1/h_2=0.1, a_2/h_2=0.4, h_1/h_2=0.7, b_1/h_2=1.25, b_3/h_2=1.75, h_3/h_2=0.6, \theta=\frac{\pi}{4}, M/h_2^2=1.5$ against wave number Kh_2 that satisfy the energy identity given by $|R|^2+\mathcal{J}|T|^2=1$. This is a check on the correctness of all the numerical results obtained for the reflection and transmission coefficients which are represented in TABLE 5.

TABLE 5. Reflection and Transmission coefficients for $a_1/h_2=0.1, a_2/h_2=0.4, h_1/h_2=0.7, b_1/h_2=1.25, b_3/h_2=1.75, h_3/h_2=0.6, \theta=\frac{\pi}{4}, M/h_2^2=1.5$.

Kh_2	$\lvert R\rvert$	$\lvert T\rvert$	$\mathcal{J}$	$\lvert R\rvert^2+\mathcal{J}\lvert T\rvert^2$
1.0	0.110915	0.981331	1.02564	1
1.25	0.106082	0.981703	1.02595	1
1.5	0.146163	0.976538	1.02623	1
1.75	0.202373	0.966691	1.02628	1
2.0	0.246970	0.956689	1.02595	1

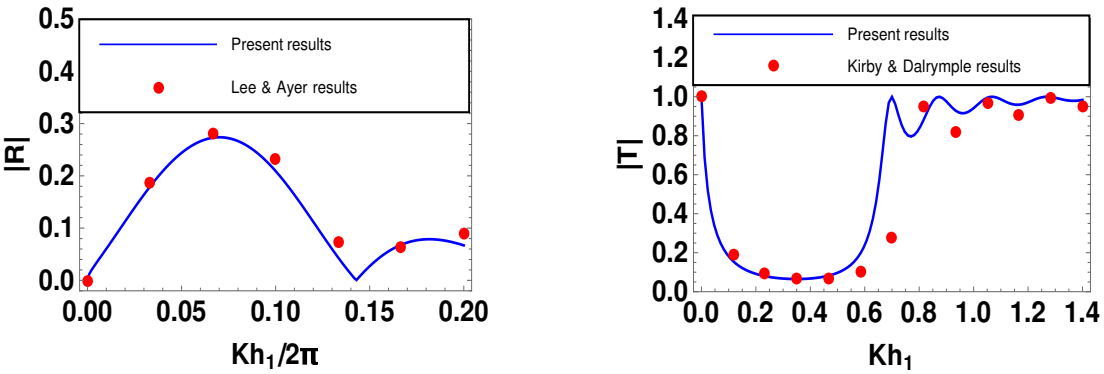

(A) (B)

FIGURE 2. (A) Reflection coefficient against $Kh_1/2\pi$ for $a_1/h_1=0.001, a_2/h_1=0.001, h_2/h_1=2, b_1/h_1=2.5, b_3/h_1=2.5, h_3=h_1, \theta=0, M/{h_1}^2=0$;
(B) Transmission coefficient vs. wave number for $a_1/h_1=0.001, a_2/h_1=0.001, h_2/h_1=3.0, b_1/h_1=5.0, b_3/h_1=5.0, h_3/h_1=1.0, \theta=0, M/h_1^2=0$.

We have compared our results with the results by Lee and Ayer [19] to check the accuracy of the numerical estimates for reflection and transmission coefficients by taking the length of the barrier so small i.e. the fully submerged barrier is almost absent and considering $a_1/h_1 = 0.001, a_2/h_1 = 0.001, h_2/h_1 = 2, b_1/h_1 = 2.5, b_3/h_1 = 2.5, h_3 = h_1, \theta = 0, M/{h_1}^2 = 0$. Now $|R|$ are plotted against the ratio of the depth of water and incident wave length ($Kh_1/2\pi = h/\lambda$) in FIGURE 2(A). It is seen that these graphs almost coincides for symmetric trench with the graphs of FIGURE 2(A) in Lee and Ayer [19] corresponding to $|R|$. The coincidence of dots on the solid lines validates the correctness of the method.

FIGURE 2(B) displays a comparison between our present results and the results by Kirby and Darlymple [16] that has been established for no fully submerged barrier is present by taking $a_1/h_1 = 0.001, a_2/h_1 = 0.001$ so small. Due to the set of values $a_1/h_1 = 0.001, a_2/h_1 = 0.001, h_2/h_1 = 3.0, b_1/h_1 = 5.0, b_3/h_1 = 5.0, h_3/h_1 = 1.0, \theta = 0, M/h_1^2$, the rigid barrier with trench problem is almost converted to simply a trench problem. The dots in Figure 3 represent the results of Kirby and Darlymple [16] and the coincidence of dots on the graphs corresponding to our results again validates the correctness of the present method.

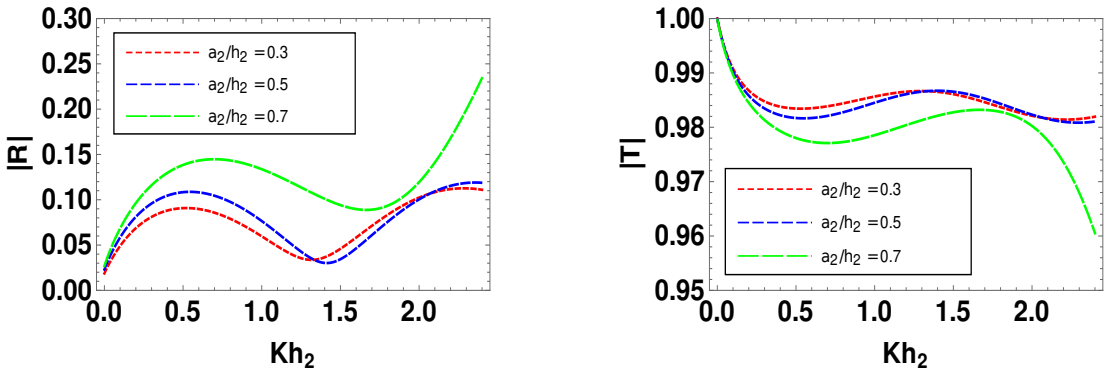

(A) (B)

FIGURE 3. (A) Reflection, (B) Transmission coefficients vs. wave number for different a_2/h_2 with $a_1/h_2 = 0.2, h_1/h_2 = 0.7, h_3/h_2 = 0.6, b_1/h_2 = 0.5, b_3/h_2 = 0.75, \theta = \frac{\pi}{4}, M/{h_2}^2 = 1.5$.

FIGURE 3 depict $|R|$ and $|T|$ respectively, against Kh_2 for different values of a_2/h_2 and $a_1/h_2 = 0.2, h_1/h_2 = 0.7, h_3/h_2 = 0.6, b_1/h_2 = 0.5, b_3/h_2 = 0.75, \theta = \frac{\pi}{4}, M/{h_2}^2 = 1.5$. Here, the position of the barrier is fixed at $a_1/h_2 = 0.2$ but the length of the barrier a_2/h_2 varies. It is observed that, $|R|$ starts from nearer to zero against Kh_2 for small waves, then begin to increase as Kh_2 increases. Similarly, in FIGURE 3(B), $|T|$ starts nearer to unity for small waves, then begins to decrease as Kh_2 increases. FIGURE 3(A) shows that $|R|$ gradually decreases as the length of the barrier decreases but opposite behavior is observed for $|T|$ in FIGURE 3(B).

In FIGURE 4, reflection and transmission coefficients are depicted against wave number Kh_2 for different angles of incident with $a_1/h_2 = 0.1, a_2/h_2 = 0.5, b_1/h_2 = 1.25, b_3/h_2 = 1.5, h_1/h_2 = 0.65, h_3/h_2 = 0.55, M/h_2^2 = 1.5$. Initially, $|R|$ increases and $|T|$ decreases with increasing values of angle of incidence. When values of θ are almost 90^0, reflection coefficient is almost unity and the transmission coefficients almost vanishes.

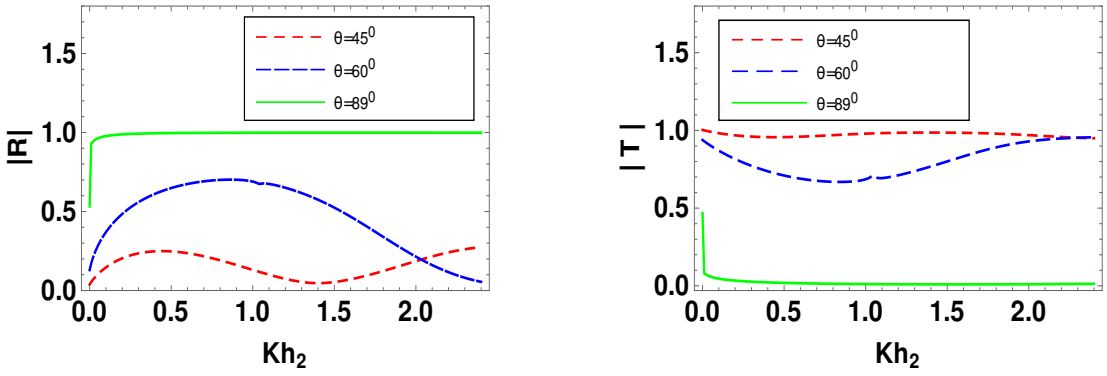

(A) (B)

FIGURE 4. (A) Reflection, (B) Transmission coefficients vs. wave number for different angle of incidence with $a_1/h_2 = 0.1, a_2/h_2 = 0.5$, $b_1/h_2 = 1.25, b_3/h_2 = 1.5$, $h_1/h_2 = 0.65, h_3/h_2 = 0.55, M/h_2^2 = 1.5$.

In FIGURE 5, the behavior of $|R|$ and $|T|$ against Kh_2 with set of values for different width of barrier with $a_1/h_2 = 0.15, a_2/h_2 = 0.45, h_1/h_2 = 0.65, h_3/h_2 = 0.55, \theta = \frac{\pi}{3}, M/{h_2}^2 = 1$ are dipcted. In FIGURE 5(A), $|R|$ is observed that it first increase and then gradually decrease as the wave number increases. An oscillatory nature has occurred and with the increasing values of width, it oscillates more. A contrasting behavior is seen for transmission coefficients. As the width of the trench becomes larger, it reflects wave more and transmit less.

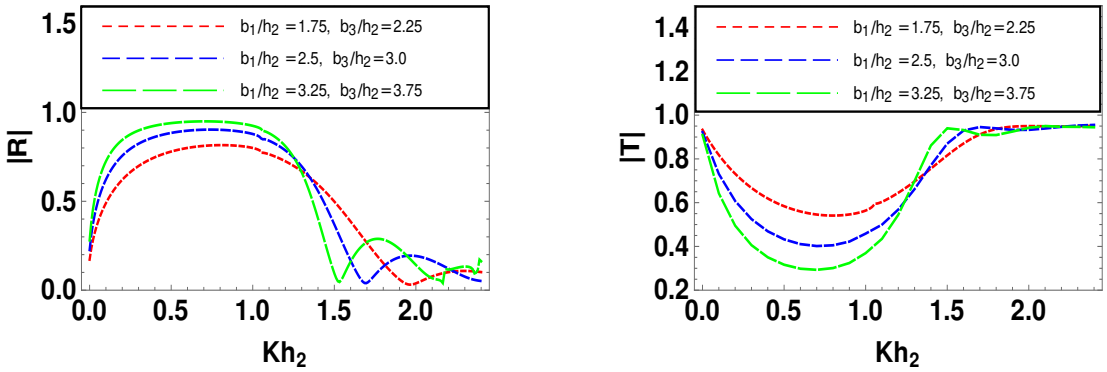

(A) (B)

FIGURE 5. (A) Reflection, (B) Transmission coefficients vs. wave number for different width of trench with $a_1/h_2 = 0.15, a_2/h_2 = 0.45, h_1/h_2 = 0.65, h_3/h_2 = 0.55, \theta = \frac{\pi}{3}, M/{h_2}^2 = 1$.

In FIGURE 6(A), $|R|$ is depicted against Kh_2 for different values of depths before and after asymmetrical trench and fixing depth of the trench by varing $h_1/h_2 (= 0.70, 0.75, 0.80)$ and $h_3/h_2 (= 0.60, 0.65, 0.75)$ while $a_1/h_2 = 0.1, a_2/h_2 = 0.4, b_1/h_2 = 0.75, b_3/h_2 = 0.5, \theta = \frac{\pi}{4}, M/{h_2}^2 = 1.5$ are kept fixed. It is seen that, $|R|$ starts from nearer to zero for Kh_2 near zero, slightly increases at first as Kh_2 increases and then quickly decreases and again begins to increase as Kh_2 further increases. Here, the wave energy is reflected back for some value of Kh_2 depending on the depths of trench. In FIGURE 6(B), $|T|$

starts from unity when Kh_2 is nearer to zero, then it increases as Kh_2 increases. Here, wave energy is transmitted less as the depths of the trench increased.

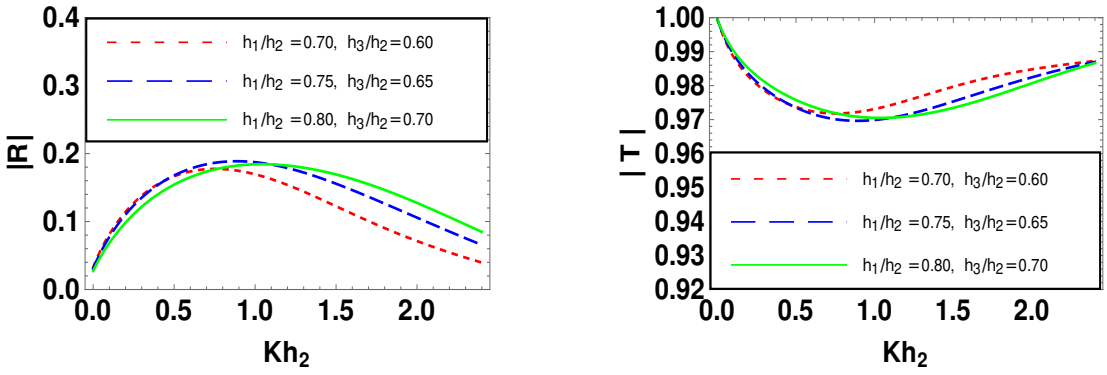

(A) (B)

FIGURE 6. (A) Reflection, (B) Transmission coefficients vs. wave number for different depth of trench with $a_1/h_2 = 0.1, a_2/h_2 = 0.4, b_1/h_2 = 0.75, b_3/h_2 = 0.5, \theta = \frac{\pi}{4}, M/{h_2}^2 = 1.5$.

In FIGURE 7, the effects of surface tension on reflection, transmission coefficients and wave load are shown in respectively. A similar patterns of the curves is observed for all the different values of $M/h_2^2 = 0.5, 1.0, 1.5$. From the FIGURES 7(A),7(B) an oscillatory behavior are seen. It is observed that the values of reflection coefficients decreases as the surface tension increases. Its occur because of the phenomena that the cohesive force between fluid molecules at the free surface. Thus in presence of surface tension, more energy is transmitted and less energy is reflected. In FIGURE 7(C), it is seen from the graph that for small values of wavenumber, the wave load on the barrier increases very slightly as the surface tension parameter increases but for large values of wavenumber, an opposite trend is noticed. The effect of surface tension becomes dominant for higher wave frequencies which is capable to reduce the force on the barrier.

In FIGURE 8, three curves of $|R|$ with different depth ratios before and after trench ($h_1 > h_3$, $h_1 = h_3$ and $h_1 < h_3$) are plotted to fix the depths of trench from free surface. Here, the incident wave direction is from negative infinity of the x-axis. Due to asymmetric trench, zero reflection has not occurred in the cases of $h_1 > h_3$ and $h_1 < h_3$. But in case of symmetric trench, $h_1 = h_3$ zero reflection occurred for $Kh_3 = 0, 1.6$ In figure, it is seen that in starting $|R|$ increases as the wave number increases. After reaching a peak value between 0.6 and 0.8, it again decreases. When $h_1/h_3 > 1$, amount of reflected energy is less in comparison to the other cases.

4.3. **Case II: The barrier on the right side of the trench.** For the second position, where the fully submerged barrier is placed on the right side from the position $x = 0$ of the trench ($x = b_2 < b_3$). We also seen that the numerical estimates for the reflection and transmission coefficients satisfy the energy identity $|R|^2 + \mathcal{J}|T|^2 = 1$ where $\mathcal{J}$ is always a positive non-zero real number. TABLE 6 displays the estimates of $|R|^2 + \mathcal{J}|T|^2 = 1$ for different values of Kh_2. Therefore, TABLE 6 validates the correctness of the method used here.

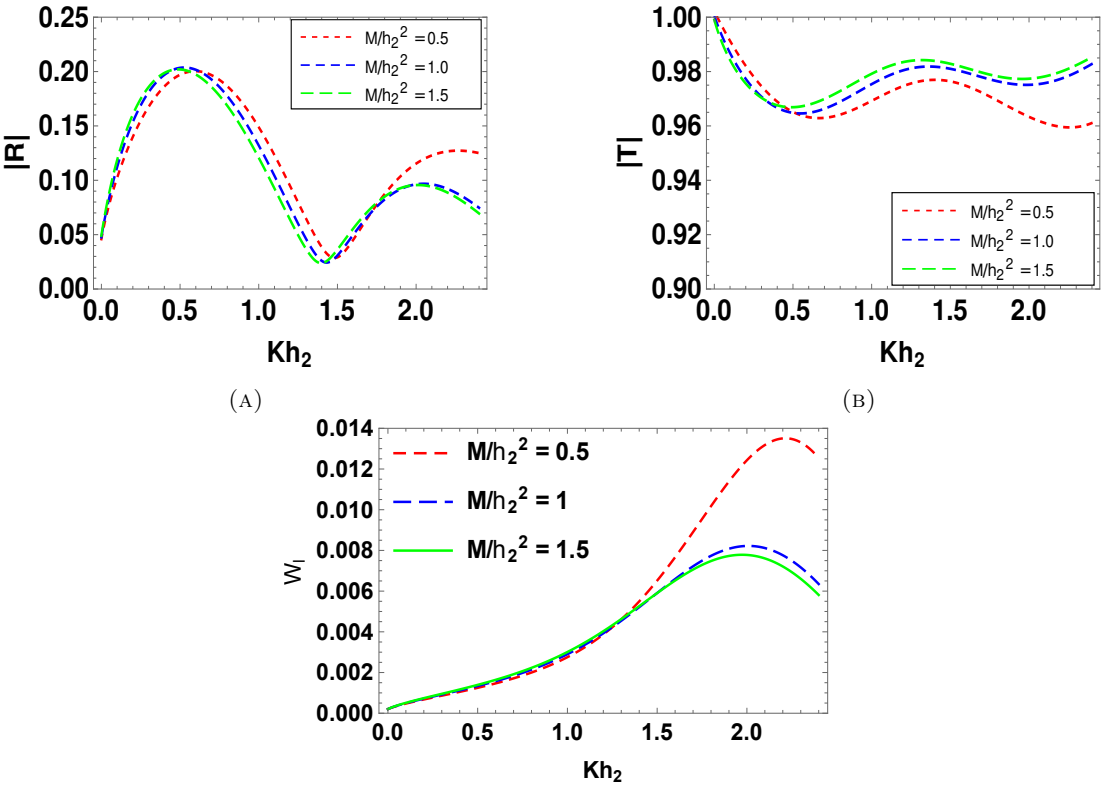

FIGURE 7. Reflection, Transmission coefficients, wave load vs. wave number for different surface tension with $a_1/h_2 = 0.15, a_2/h_2 = 0.45,\ \ b_1/h_2 = 0.75, b_3/h_2 = 1.25, h_1/h_2 = 0.65, h_3/h_2 = 0.55,\ \ \theta = \frac{\pi}{4}$.

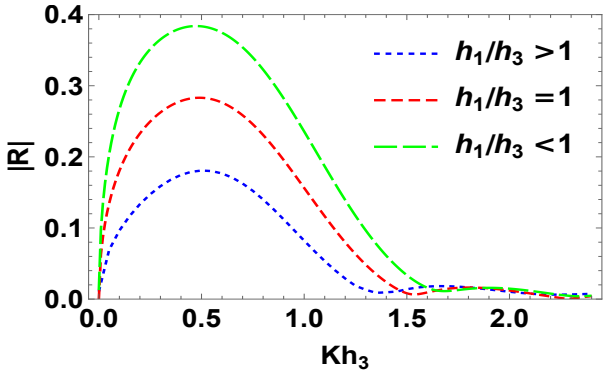

FIGURE 8. Reflection coefficient vs. wave number with $a_1/h_3 = 0.2, a_2/h_3 = 0.5, b_1/h_3 = 0.75, b_3/h_3 = 1.25, h_2/h_3 = 2.5,\ \ \theta = \frac{\pi}{4}$.

The behaviors of $|R|$ and $|T|$ are against Kh_2 shown in FIGURE 9 by varying the length of the barriers and fixing upper position of barrier with set of values $a_1/h_2 = 0.1, b_1/h_2 = 1.25, b_2/h_2 = 0.5, b_3/h_2 = 0.75, h_1/h_2 = 0.55, h_3/h_2 = 0.65, \theta = \frac{\pi}{4}, M/{h_2}^2 = 1.5$. It is observed in FIGURE 9(A) that $|R|$ increases as the length of barriers increases. An opposite behavior is seen for $|T|$ in FIGURE 9(B).

TABLE 6. Reflection and Transmission coefficients for $a_1/h_2 = 0.15, a_2/h_2 = 0.45, h_1/h_2 = 0.65, b_1/h_2 = 0.75, b_2/h_2 = 0.75, b_3/h_2 = 1.25, h_3/h_2 = 0.7, \theta = \frac{\pi}{4}, M/{h_2}^2 = 1$.

Kh_2	$\lvert R\rvert$	$\lvert T\rvert$	$\mathcal{J}$	$\lvert R\rvert^2 + \mathcal{J}\lvert T\rvert^2$
1.0	0.136293	0.976015	1.03025	1
1.25	0.0932005	0.980824	1.03045	1
1.5	0.0982835	0.980295	1.03056	1
1.75	0.125425	0.977327	1.03047	1
2.0	0.128747	0.977089	1.03008	1

As the lengths of the barrier increases, the wave energy reflected more, and transmitted less.

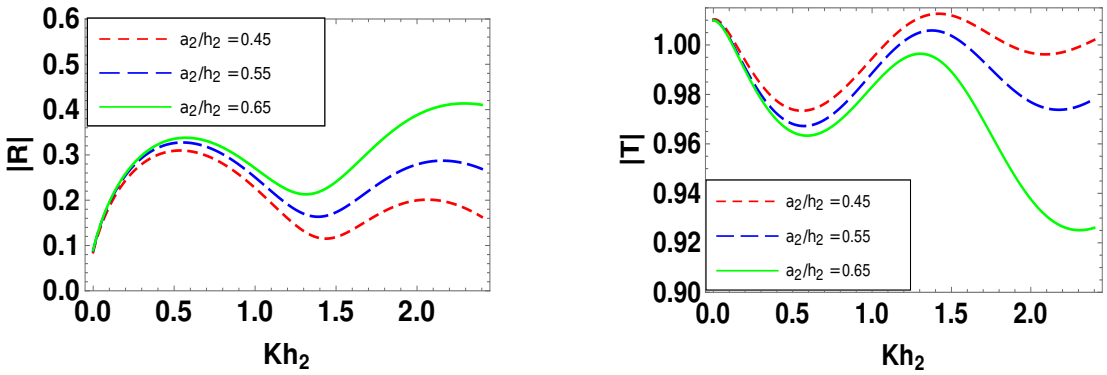

(A) (B)

FIGURE 9. (A) Reflection, (B) Transmission coefficients vs. wave number for different lengths of barrier with $a_1/h_2 = 0.1, b_1/h_2 = 1.25, b_2/h_2 = 0.5, b_3/h_2 = 0.75, h_1/h_2 = 0.55, h_3/h_2 = 0.65, \theta = \frac{\pi}{4}, M/{h_2}^2 = 1.5$.

The FIGURE 10(A) demonstrated how $|R|$ acts when the fully submerged barrier is shifted gradually to the right from the position $x = 0$ of the trench. Here, $|R|$ is plotted against Kh_2 for different positions setting the values of $b_2/h_2(= 0.25, 0.50, 0.75)$ and $a_1/h_2 = 0.15, a_2/h_2 = 0.45, b_1/h_2 = 0.75, b_3/h_2 = 1.0, h_1/h_2 = 0.65, h_3/h_2 = 0.55, \theta = \frac{\pi}{4}, M/{h_2}^2 = 1$ i.e. $b_2 < b_3$. Here, $|R|$ increases very slowly from near to zero for close to $Kh_2 = 0$ in all the cases, after that it decreases$(0.45 < Kh_2 < 1.35)$. Then $|R|$ increases again as Kh_2 increases. We have seen that reflection becomes maximum peak when the barrier is placed at $b_2/h_2 = 0.75$. In FIGURE 10(B), the behavior of $|T|$ is observed for the similar condition which is used for FIGURE 10(B). Here, $|T|$ starts from unity near $Kh_2 = 0$ in all the cases and then decreases slightly as Kh_2 increases and then increasing a little, after that it decreases again. These two figures unveil that amount of reflected energy increases as the barrier will be close to side of trench, whereas an opposite behavior is observed for transmission coefficient.

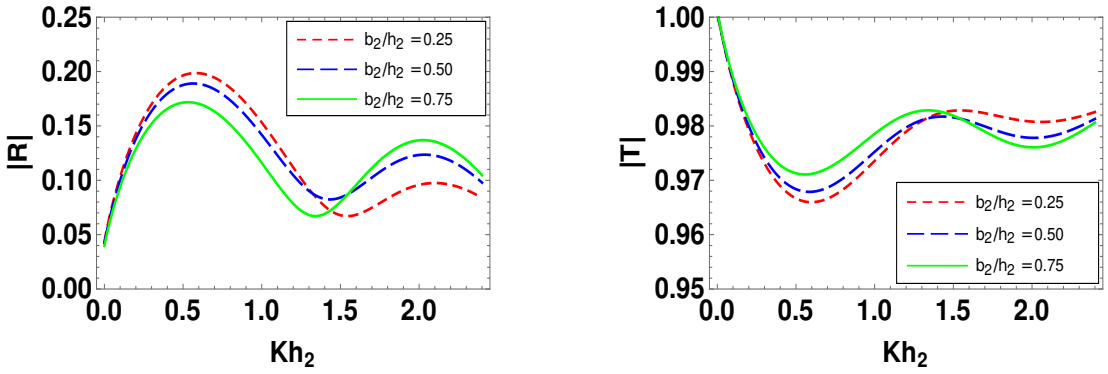

(A) (B)

FIGURE 10. (A) Reflection, (B) Transmission coefficients vs. wave number for different positions of barrier with $a_1/h_2 = 0.15, a_2/h_2 = 0.45, b_1/h_2 = 0.75, b_3/h_2 = 1.0, h_1/h_2 = 0.65, h_3/h_2 = 0.55, \theta = \frac{\pi}{4}, M/{h_2}^2 = 1$.

In FIGURE 11, $|R|$ and $|T|$ are plotted against Kh_2 by taking different width of trench. Three curves are depicted in each figure for different values of width of the trench with $a_1/h_2 = 0.15, a_2/h_2 = 0.55, b_1/h_2 = 0.5, b_2/h_2 = 0.65, b_3/h_2 = 1.0, h_1/h_2 = 0.65, h_3/h_2 = 0.55, \quad \theta = \frac{\pi}{4}, M/{h_2}^2 = 1$. These two figures reveal that amount of reflection increases as width of the trench decreases whereas an opposite behavior is observed for transmission coefficient.

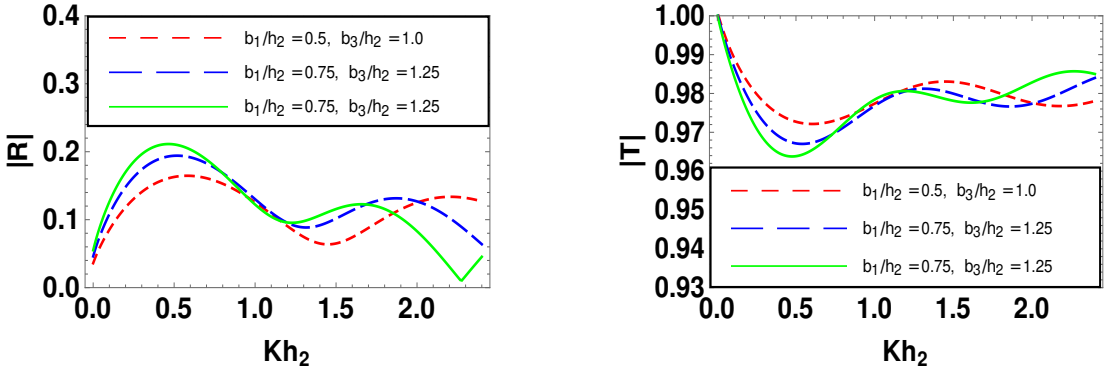

(A) (B)

FIGURE 11. (A) Reflection, (B) Transmission coefficients vs. wave number for different width of trench with $a_1/h_2 = 0.15, a_2/h_2 = 0.55, b_2/h_2 = 0.65, h_1/h_2 = 0.65, h_3/h_2 = 0.55, \theta = \frac{\pi}{4}, M/{h_2}^2 = 1$.

The effects of surface tension on reflection, transmission coefficients and wave load are plotted in FIGURES 12(A),(B),(C) respectively with the set of values $a_1/h_2 = 0.1, a_2/h_2 = 0.4, \quad b_1/h_2 = 1.5, b_3/h_2 = 2.0, h_1/h_2 = 0.7, h_3/h_2 = 0.6, \quad \theta = \frac{\pi}{4}$. From FIGURES 12(A),(B), an oscillatory behavior is seen. It is observed that the values of reflection coefficients decreases as the surface tension increases. The free surface of the fluid feels stretched as the inter molecular force increases with the surface tension. Hence, in presence of surface tension, more energy is transmitted and less energy is reflected. In FIGURE 12(C), the wave load on the barrier increases initially as the surface tension parameter increases for

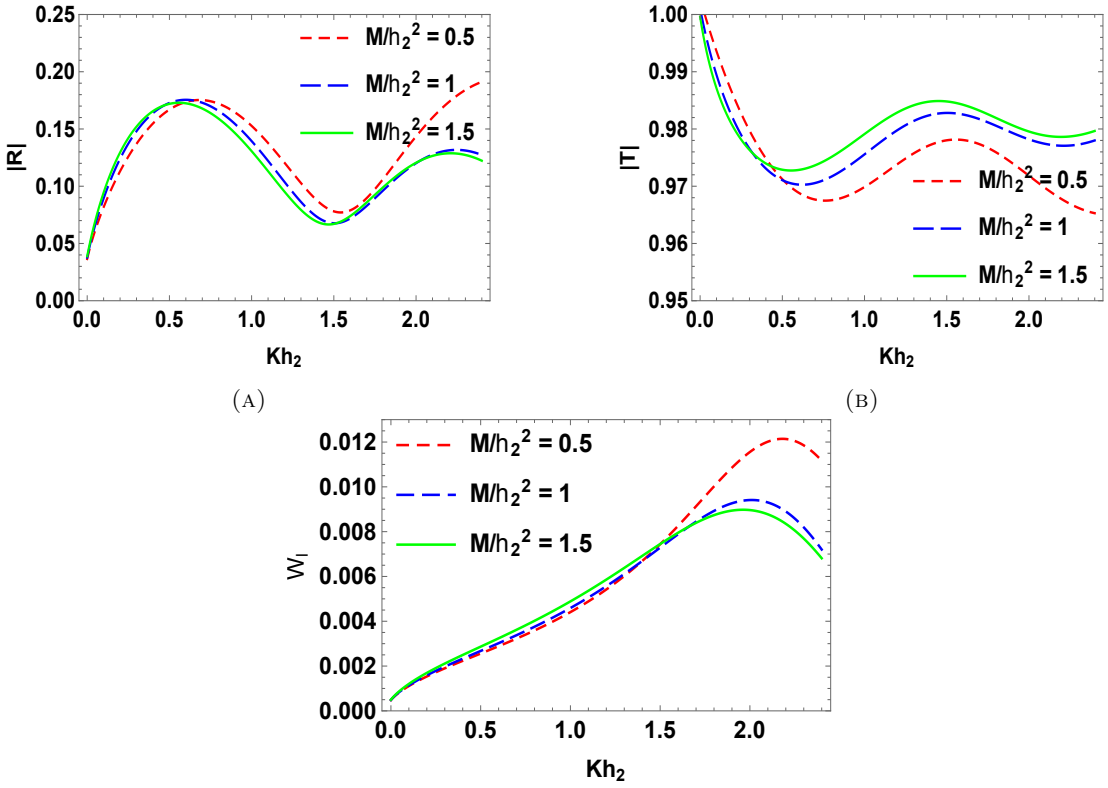

FIGURE 12. (A) Reflection, (B) Transmission coefficients, (C) wave load vs. wave number for different surface tension with $a_1/h_2 = 0.15, a_2/h_2 = 0.55,\ b_1/h_2 = 0.5, b_2/h_2 = 0.65, b_3/h_2 = 1.0, h_1/h_2 = 0.65, h_3/h_2 = 0.55,\ \theta = \frac{\pi}{4}$.

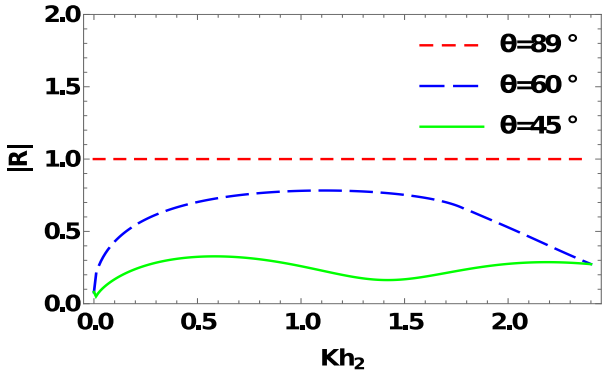

FIGURE 13. Reflection coefficient vs. wave number for different theta with $a_1/h_2 = 0.1, a_2/h_2 = 0.55, b_1/h_2 = 1.25, b_2/h_2 = 0.5, b_3/h_2 = 0.75, h_1/h_2 = 0.55, h_3/h_2 = 0.65, M/{h_2}^2 = 1.5$.

small values of wavenumber, but for large values of wavenumber, an opposite behavior is observed.

In FIGURE 13, reflection coefficients is depicted against wave number Kh_2 for different angle of incident with $a_1/h_2 = 0.1, a_2/h_2 = 0.55, b_1/h_2 = 1.25, b_2/h_2 = 0.5, b_3/h_2 = 0.75, h_1/h_2 = 0.55, h_3/h_2 = 0.65, M/{h_2}^2 = 1.5$. Initially, $|R|$ increases with increasing values of angle of incidence. When values of θ almost 90^0, there are no transmitted wave energy. From the figure, it is clear that present result satisfy the geometry of the problem.

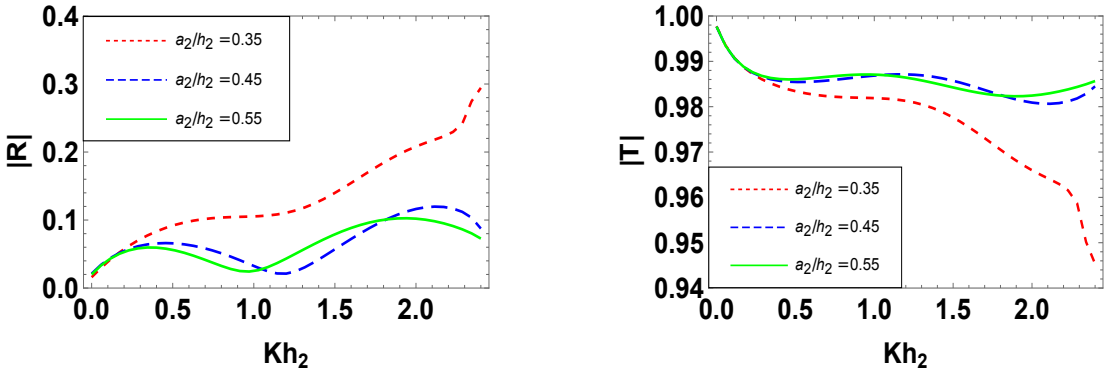

(A) (B)

FIGURE 14. (A) Reflection, (B) Transmission coefficients vs. wave number for different length of barrier with $b_1/h_2 = 0.75, b_2/h_2 = 1.25, b_3/h_2 = 1.0, h_1/h_2 = 0.75, h_3/h_2 = 0.65$, $a_1/h_2 = 0.15, \theta = \frac{\pi}{4}, M/{h_2}^2 = 1.5$.

4.4. **Case-III: The barrier is shifted outside of the trench.** For the third position, where the fully submerged barrier is shifted outside of the trench ($x = b_3 < b_2$). We also observe that the numerical estimates for the reflection and transmission coefficients satisfy the energy identity $|R|^2 + \mathcal{J}|T|^2 = 1$. $|R|$ and $|T|$ are plotted against Kh_2 in Figure 14 by varying the length of the barriers and adjusting the upper position of the barrier with the set of values $a_1/h_2 = 0.15, b_1/h_2 = 0.75, b_2/h_2 = 1.25, b_3/h_2 = 1.0, h_1/h_2 = 0.75, h_3/h_2 = 0.65, \theta = \frac{\pi}{4}, M/{h_2}^2 = 1.5$. In FIGURE 14(A), it is seen that $|R|$ increases as the barrier length increases. An opposite pattern is seen for $|T|$ in FIGURE 14(B). The interaction between barrier and surface waves, the wave energy is reflected, more, and transmitted less, as the barrier length increases.

FIGURE 15 explain how $|R|, |T|$ act when the fully submerged barrier is gradually shifted outside the trench. Here, $|R|, |T|$ are plotted against Kh_2 for different positions setting the values of $b_2/h_2 (= 1.5, 1.57, 2.25)$ and $a_1/h_2 = 0.15, a_2/h_2 = 0.55, b_1/h_2 = 0.75, b_3/h_2 = 1.25, h_1/h_2 = 0.7, h_3/h_2 = 0.6, \theta = \frac{\pi}{4}, M/{h_2}^2 = 1.5$, that is, $b_3 < b_2$. Here, $|R|$ increases very slowly for close to $Kh_2 = 0$ in all cases, after which it decreases. Then $|R|$ increases again as Kh_2 increases. We have seen that the reflection becomes large when the thin barrier is very close to the trench. In FIGURE 15(B), $|T|$ starts from unity near $Kh_2 = 0$ in all cases and then decreases slightly as Kh_2 increases and then increases a little, after which it decreases again. This figure reveals that the amount of transmitted energy decreases as the barrier is close to the side of the trench.

The effects of surface tension on reflection, transmission coefficients and wave load are shown in FIGURES 16(A),(B),(C), respectively with the set of values $a_1/h_2 = 0.15, a_2/h_2 = 0.55, b_1/h_2 = 0.5, b_2/h_2 = 1.25, b_3/h_2 = 1.0, h_1/h_2 = 0.65, h_3/h_2 = 0.55, \theta = \frac{\pi}{4}$. In FIGURES 16(A),(B),(C) an oscillatory behavior is seen. It is observed that the amount of reflected energy decreases and the

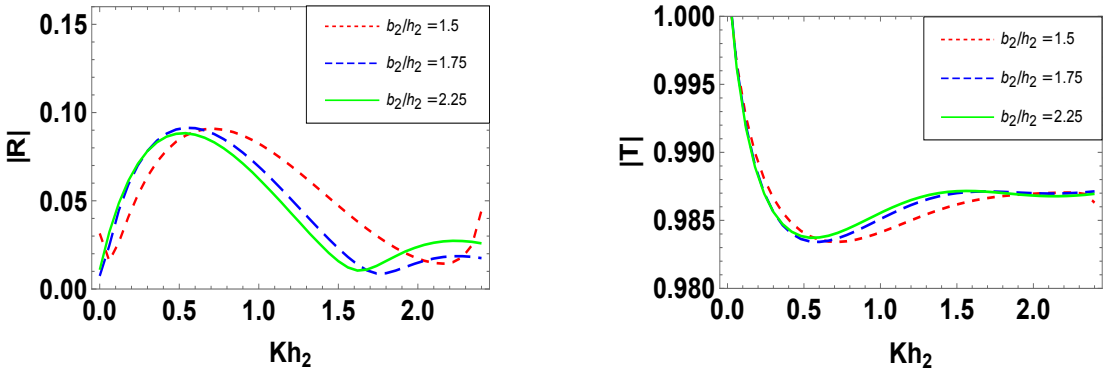

(A) (B)

FIGURE 15. (A) Reflection, (B) Transmission coefficients vs. wave number for different position of barrier with $a_1/h_2 = 0.15, a_2/h_2 = 0.55$, $b_1/h_2 = 0.75, b_3/h_2 = 1.25, h_1/h_2 = 0.7, h_3/h_2 = 0.6$, $\theta = \frac{\pi}{4}, M/{h_2}^2 = 1.5$.

transmitted energy increases as the surface tension increases. Whenever the surface tension increases, that increases the intermolecular force acting between fluid particles. Therefore, the free surface of the fluid feels stretched, causing more transmission and less reflection. In FIGURE 16(C), the wave load on the barrier decreases as the surface tension parameter increases.

The comparison between the three cases depending on the different positions of the barrier is shown in FIGURE 17. In the figure, the reflection coefficient is plotted against the wave number with the set of values $a_1/h_2 = 0.15, a_2/h_2 = 0.55, b_1/h_2 = 0.5, b_2/h_2 = 1.25, b_3/h_2 = 1.0, h_1/h_2 = 0.65, h_3/h_2 = 0.55$, $\theta = \frac{\pi}{4}$. For the first case, the barrier position is $b_2/h_2 = 0$, in second case it is $b_2/h_2 = 0.45$ and in third case $b_2/h_2 = 1.25$. Now, it is observed from the figure that for small values of the wave number, $|R|$ decreases when the barrier is shifted towards the wall of the trench. In addition, the barrier placed outside the trench shows minimum reflection. But with increasing values of the wave number, $|R|$ becomes larger for case III than the case II and I. For $Kh_2 > 1.5$ these opposite behaviors are clearly visible. Thus, for small wave numbers Case I barrier is more suitable and with larger wave number case III barrier reflects more energy so it becomes more appropriate than the others.

5. Conclusion

The interaction of oblique waves by fully submerged thin vertical barrier in presence of surface tension over an asymmetric trench for different three positions, are discussed in this paper based assuming the linear potential theory. At first, the problem is reduced to first kind integral equations involving horizontal component of velocity. It has different types of singularity such as cube-root singularity at the edges of trench and square-root singularity for rigid barrier at the end points, which are solved by using two different methods, which are the boundary element method(BEM) and the multi-term Galerkin method along with appropriate basis functions. Here we consider two different types of basis functions, one is simple polynomials [30] and another is orthogonal polynomials such as Gegenbauer polynomial of order $\frac{1}{6}$ and Chebychev polynomials, multiplied by appropriate weight functions respectively. In multi-term Galerkin method, taking these polynomial form of the first kind integral equations, they become more easier to operate. The solutions are obtained in terms of Bessel functions and modified Bessel functions of 1st kind, which are quite easy for numerical calculations and give better convergence rate with the comparison of choosing simple polynomial as a basis function. This method also provides a procedure

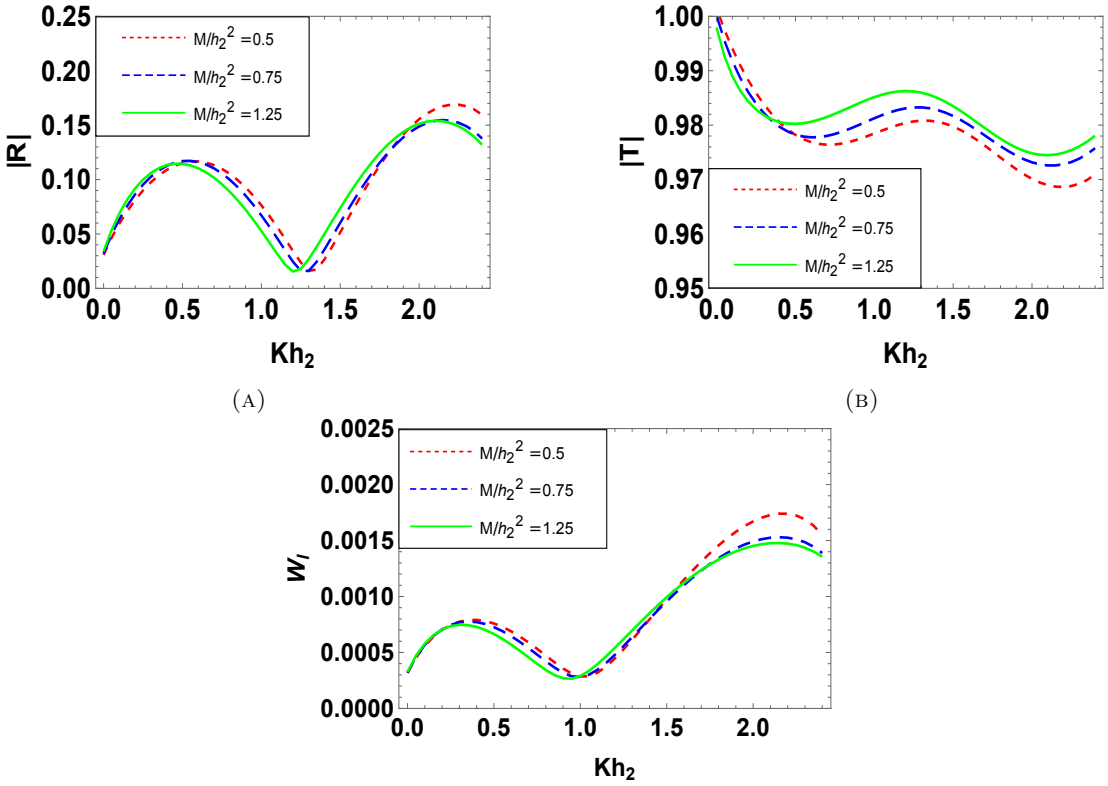

FIGURE 16. Reflection, Transmission coefficients, wave load vs. wave number for different surface tension with $a_1/h_2 = 0.15$, $a_2/h_2 = 0.55$, $b_1/h_2 = 0.5$, $b_2/h_2 = 1.25$, $b_3/h_2 = 1.0$, $h_1/h_2 = 0.65$, $h_3/h_2 = 0.55$, $\theta = \frac{\pi}{4}$.

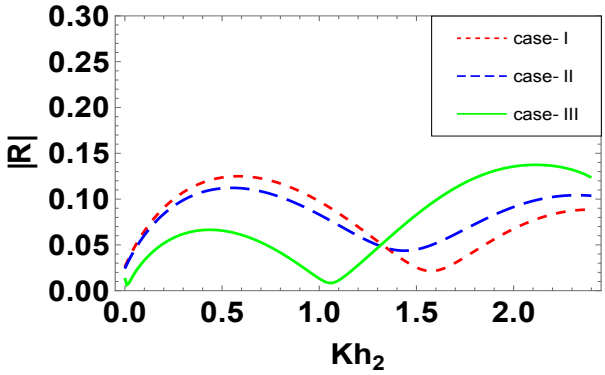

FIGURE 17. Reflection coefficient vs. wave number for three cases with $a_1/h_2 = 0.1$, $a_2/h_2 = 0.4, b_1/h_2 = 0.5, b_3/h_2 = 0.75, h_1/h_2 = 0.7, h_3/h_2 = 0.6, M/{h_2}^2 = 1.5, \theta = \frac{\pi}{4}$.

for handling wave interaction problem involving various edge conditions with different ordered such as one-third, half, and other singularities. In the present study, very accurate numerical estimations for reflection and transmission coefficients are obtained which satisfy the energy identity and wave load acting on the barrier which are also evaluated. The numerical results are demonstrated in a number of

figures that some of the figures match quite well with previous work. The position and length of the barrier, angle of incidence, and width of trench in presence of surface tension impact significantly on the wave reflection and transmission. When the length of fully submerged barrier increased, it reflect wave energy more and transmit less. When the width of trench become larger, it transmit more energy. Thus, submerged structures are suitable choice for complete protection from waves. Such structures are beneficial over conventional type structures incorporating lower maintenance costs, controlled marine ecosystem, etc. It is also observed that how surface tension controlling the reduction of wave force which is acted on the barrier for higher wave frequency.

6. Nomenclature

- $a_2 - a_1$- length of the partially immersed barrier
- $b_3 + b_1$ - width of the trench
- h_2- depth of the trench from the free surface
- h_1 and h_3- depth of the uniform fluid region outside of the trench
- l- distance of the barrier from the middle of the trench on the free surface
- M- coefficient of surface tension σ- angular frequency of incoming wave train
- R, T- Reflection and Transmission coefficients
- ϕ^{inc}-velocity potential of the incident wave
- r_1-distance from the submerged edge of the trench
- r_2 - distance from the submerged sharp edge of the barrier

References

[1] C. J. Bender, R. G. Dean, *Wave transformation by two-dimensional bathymetric anomalies with sloped transitions,* Coastal Engineering, **50(1-2)**(2003), 61-84.

[2] R. Chakraborty, B. N. Mandal, *Water wave scattering by a rectangular trench,* Journal of Engineering Mathematics, **89(1)**(2014), 101-112.

[3] R. Chakraborty, B. N. Mandal, *Oblique wave scattering by a rectangular submarine trench,* The ANZIAM Journal, **56(3)**(2015), 286-298.

[4] X. B. Chen, *Role of the surface tension in modelling ship waves,* In Proc. of the 17th Inter. Workshop on water Waves and floating bodies, edited by RC Rayney and SF Lee, Peterhouse Cambridge, UK, 2002, pp. 14-17.

[5] D. V. Evans, *The influence of surface tension on the reflection of water waves by a plane vertical barrier,* In Mathematical Proceedings of the Cambridge Philosophical Society. Cambridge University Press. **64(3)**(1968), 795-810.

[6] D.V. Evans, *Diffraction of water waves by a submerged vertical plate,* Journal of Fluid Mechanics. **40(3)**(1970), 433-451.

[7] D. V. Evans, C. A. N. Morris, *The effect of a fixed vertical barrier on obliquely incident surface waves in deep water,* IMA Journal of Applied Mathematics. **9(2)**(1972), 198-204.

[8] D. V. Evans, M. Fernyhough, *Edge waves along periodic coastlines. Part 2,* Journal of Fluid Mechanics. **297**(1995), 307-325.

[9] T. H. Havelock, *Forced surface-waves on water.*The London, Edinburgh, and Dublin Philosophical Magazine and Journal of Science. **8(51)**(1929), 569-576.

[10] S. J. Hogan, *Some effects of surface tension on steep water waves.* Journal of Fluid Mechanics, **91(1)**(1979), 167-180.

[11] T. H. Jung, K.D. Suh, S.O. Lee, and Y. S. Cho, *Linear wave reflection by trench with various shapes.* Ocean Engineering. **35(11-12)**(2008), 1226-1234.

[12] M. Kanoria, D. P. Dolai, and B.N. Mandal, *Water-wave scattering by thick vertical barriers,* Journal of engineering mathematics, **35**(1999), 361-384.

[13] P. Kar, S. Koley, and T. Sahoo, *Scattering of surface gravity waves over a pair of trenches,* Applied Mathematical Modelling, **62**(2018), 303-320.

[14] A. Kaur, S. C. Martha, and A. Chakrabarti, *Solution of the problem of propagation of water waves over a pair of asymmetrical rectangular trenches,* Applied Ocean Research, **93**(2019):101946.

[15] A. Kaur, S. C. Martha, and A. Chakrabarti, *Linear algebraic method of solution for the problem of mitigation of wave energy near seashore by trench-type bottom topography,* Journal of Engineering Mechanics, **146(11)**(2020): 04020125.
[16] J. T. Kirby, R.A. Dalrymple, *Propagation of obliquely incident water waves over a trench,* Journal of Fluid Mechanics, **133**(1983), 47-63.
[17] G. Kreisel, *Surface waves,* Quarterly of Applied Mathematics, **7(1)**(1949), 21-44.
[18] J. B. Lassiter, *The propagation of water waves over sediment pockets* (Doctoral dissertation, Massachusetts Institute of Technology), 1972.
[19] J. J. Lee, R. M. Ayer, *Wave propagation over a rectangular trench,* Journal of fluid mechanics, **110**(1981), 335-347.
[20] H. W. Liu, D. J. Fu, and X. L. Sun, *Analytic solution to the modified mild-slope equation for reflection by a rectangular breakwater with scour trenches,* Journal of Engineering Mechanics, **139(1)**(2013), 39-58.
[21] S. R. Manam, J. Bhattacharjee, and T. Sahoo, *Expansion formulae in wave structure interaction problems,* Proceedings of the Royal Society A: Mathematical, Physical and Engineering Sciences, **462(2065)**(2006), 263-287.
[22] C. C. Mei, J. L. Black, *Scattering of surface waves by rectangular obstacles in waters of finite depth,* Journal of Fluid Mechanics, **38(3)**(1969), 499-511.
[23] J. W. Miles, *On surface-wave diffraction by a trench,* Journal of Fluid Mechanics, **115**(1982), 315-325.
[24] P. A. Milewski, J. M. Vanden-Broeck, *Time dependent gravity-capillary flows past an obstacle.* Wave Motion, **29(1)**(1999), 63-79.
[25] N. F. Parsons, P. A. Martin, *Scattering of water waves by submerged plates using hypersingular integral equations,* Applied Ocean Research, **14(5)**(1992), 313-321.
[26] N. F. Parsons, P. A. Martin, *Scattering of water waves by submerged curved plates and by surface-piercing flat plates,* Applied Ocean Research, **16(3)**(1994), 129-139.
[27] R. Porter, D. V. Evans, *Complementary approximations to wave scattering by vertical barriers,* Journal of Fluid Mechanics, **294**(1995), 155-180.
[28] R. Roy, R. Chakraborty, and B.N. Mandal, *Propagation of water waves over an asymmetrical rectangular trench,* The Quarterly Journal of Mechanics and Applied Mathematics, **70(1)**(2017), 49-64.
[29] R. Roy, U. Basu, and B. N. Mandal, *Oblique water wave scattering by two unequal vertical barriers,* Journal of Engineering Mathematics, **97**(2016), 119-133.
[30] S. Ray, S. De, and B.N. Mandal, *Wave propagation over a rectangular trench in the presence of a partially immersed barrier,* Fluid Dynamics Research, **53(3)**(2021): 035509.
[31] P. F. Rhodes-Robinson, *The effect of surface tension on the scattering of waves by a partially immersed vertical barrier in water of infinite depth,* Mathematika, **43(1)**(1996), 182-197.
[32] A. Samanta, R. Chakraborty, and S. Banerjea, *Line element method of solving singular integral equations,* Indian Journal of Pure and Applied Mathematics, **53(2)**(2022), 528-541.
[33] A. Samanta, R. Chakraborty, *Numerical Approach on Oblique Wave Scattering by a Wide Rectangular Impediment With a Vent Placed Under a Finite Depth Water Body With Ice-Covered Surface,* Journal of Offshore Mechanics and Arctic Engineering, **145(1)**(2023): 010903.
[34] B. Sarkar, R. Roy, and S. De, *Oblique wave interaction by two thin vertical barriers over an asymmetric trench,* Mathematical Methods in the Applied Sciences, **45(17)**(2022), 11667-11682.
[35] A. Sasmal, S. De, *Propagation of oblique water waves by an asymmetric trench in the presence of surface tension,* Journal of Ocean Engineering and Science, **6(2)**(2021), 206-214.
[36] J. W. Wright, *Detection of ocean waves by microwave radar; the modulation of short gravity-capillary waves,* Boundary-Layer Meteorology, **13(1)**(1978), 87-105.
[37] J. J. Xie, H. W. Liu, and P. Lin, *Analytical solution for long-wave reflection by a rectangular obstacle with two scour trenches,* Journal of Engineering Mechanics, **137(12)**(2011), 919-930.
[38] X. Zhang, *Capillary–gravity and capillary waves generated in a wind wave tank: observations and theories,* Journal of Fluid Mechanics, **289**(1995), 51-82.

Mampi Majhi, Department of Mathematics, Chakdaha college, Chakdaha, Nadia-741222, India
Email address: mampi.india.123@gmail.com

Rumpa Chakraborty, corresponding author, Department of Mathematics, Diamond Harbour Women's University, South 24 Parganas-743368, India
Email address: chak.rumpa@gmail.com